Ministry of Higher Education and Scientific Research

Mohamed Boudiaf University of M'sila

FACULTY OF TECHNOLOGY
DEPARTMENT OF ELECTRONICS
N°: 2024/……..……

FIELD: SCIENCE AND TECHNOLOGY
BRANCH: ELECTRONICS
SPECIALIZATION : MICROELECTRONICS

Thesis Presented for the Achievement of the Academic Master's Degree

Presented by:

- LEBACHI Taher

Title:

Study of solar cells based on CuO and Cu_2O absorbers using SCAPS-1D

Defended before the jury composed of:

Pr. BOURAS Mounir	Université M'sila	President
Pr. BOUCHAMA Idris	Université M'sila	Supervisor
Dr. HADJAB Moufdi	Université M'sila	Examiner

Academic Year: 2023/2024

Dedication

I dedicate this humble work to my dear father and my dear mother for encouraging me to continue this academic path. I pray to Allah to bless their lives and protect them from all evil.

To my brothers and sisters (..Oussama.. Iman.. Amira.. Mohammad..).

To all my friends at work, especially my team (Omar Hammo... Bilal Bairit... Housseyn Ziane... Omar Ziane... Yaqoub Saidi... Oussama Maamari). Great thanks to all.

To all my friends, without exception, and my classmates.

Lebachi Taher

Acknowledgement

*First and foremost, we would like to thank Almighty **ALLAH** for strength and patience, and for granting us the health and patience to complete this work.*

I would like to express my appreciation to my supervisor

***Prof. BOUCHAMA Idris,** Thank you for his patience and this valuable advice.*

*I would like to express my deep gratitude to **Pr. BOURAS Mounir** and **Dr. HADJAB Moufdi** who agreed to be part of our discussion comity And I gratefully acknowledge to **Dr. Marc Burgelman**, for providing the SCAPS simulation software.*

. I express my sincere thanks to them.

I would like to thank all my friends who help me directly or indirectly in carrying out this work as well as all our teachers from the Electronics Department University of Msila.

TABLE OF CONTENTS

GENERAL INTRODUCTION I

Chapter I: Physical properties of CuO and Cu_2O materials

I.1. Introduction 02

I.2. Basics of material science 02

I.2.1. Presentation of CuO and Cu_2O compounds 02

I.2.2. Chemical and physical properties of CuO and Cu_2O materials 05

I.3. In-depth Analysis of CuO 07

I.3.1. Structure and Stability 07

I.3.2. Electronic and optical properties 08

I.3.3. Mechanical and Thermal Property 09

I.3.4. Applications in Microelectronics 12

I.4. In-depth Analysis of Cu_2O 13

I.4.1. Structure and stability 13

I.4.2. Electronic and optical properties 14

I.4.3. Mechanical and thermal properties 15

I.4.4. Applications in microelectronics 16

I.5. Comparison between CuO and Cu_2O materials 17

I.6. Conclusion 17

References 18

Chapter II: Presentation of SCAPS-1D simulator

II.1. Introduction 22

II.2. Different panels in SCAPS-1D program 23

II.2.1. Creation, modification and use a Definition File 23

II.2.2. Construction of a New Definition File or the Editing of an Existing 23

II.2.3. Rear Contact 23

II.2.4. Semiconductor layers 25

II.2.5. Defects and recombination 26

II.2.6. Interface between layers 29

II.2.7. Front Contact 30

II.3. Numerical parameters 30

II.3.1. Loading and changing an Existing Definition File 30

II.3.2. Spectrum File 31

II.3.3. Importing digital simulations 32

II.4. The Action Panel 35

II.5. Energy band panel 36

II.6. Panel of IV characteristics 38

II.7. Conclusion 41

References 42

Chapter III: Results and discussions

III.1. Introduction 44

III.2. Modeling of substrate CuO and Cu_2O soler cells 44

III.3. Physical model and simulation parameters 45

III.4. Band diagrams 47

III.5. Thickness optimization of CuO and Cu_2O absorber layers 48

III.6. Optimization of acceptor density N_A(CuO) and N_A(Cu_2O) 50

III.7. Influence of defect state density of CuO and Cu_2O absorber layers 53

III.8. Hybrid CuO/CIGS and Cu_2O/CIGS solar cells modeling 55

III.8.1. Band diagrams 57

III.8.2. Thickness optimization of CIGS absorber layer for both structures 59

III.8.3. Optimization of acceptor density N_A(CIGS) for both structures 60

III.8.4. Influence of defect state density of CIGS absorber layer for both structures 61

III.8.5. Study of Cu_2O/CuO/CIGS Hybrid solar cell as a function CIGS absorber layer thickness 62

III.9. Conclusion 63

References 63

General conclusion 67

List of Figures

Chapter I: Physical properties of CuO and Cu_2O materials

Figure I.1: Unit cell structure of cupric (CuO) and cuprous (Cu_2O) oxide 05

Figure I.2: CuO structure as crystallizes in the monoclinic C2/c space group 07

Figure I.3. Phase diagram of copper oxides calculated by the method of the equilibrium state density functional 09

Figure I.4: Electronic band structure and density of states of CuO material 09

Figure I.5: Relative thermal conductivity coefficient versus density 11

Figure I.6: Heat transfer rate (Q) of CuO 11

Figure I.7: Illustration of Cu_2O Cubic structure 13

Figure I.8: Cu 2p3/2 core-level XPS spectra of Cu_2O, Cu_4O_3, and CuO thin films 09

Chapter II: Presentation of SCAPS-1D simulator

Figure II.1: Exit window 22

Figure II.2: Rear or front contact window 24

Figure II.3: The Semi-conductor's layers. 25

Figure II.4: The interface between the layers. 29

Figure II.5: Numerical parameter window 31

Figure II.6: Illumination organization space 32

Figure II.7: The .def file export tool 33

Figure II.8: Operating point determination space. 33

Figure II.9: Parameter adjustment space. 34

Figure II.10: Convergence failure window. 35

Figure II.11: The Action panel. 36

Figure II.12: The energy band panel. 37

Figure II.13: Panel of JV characteristics 39

Figure II.14: The Batch tool. 40

Figure II.15: The tunnel effect tool. 41

Chapter III: Results and discussions

Figure III.1: Cu_2O and CuO solar cell structures 45

Figure III.2: Absorption coefficient α for both Cu2O and CuO absorber films used in the simulation. 47

Figure III.3: Band diagram for (a) CuO and (b) Cu_2O solar cells structures used in the simulation. 48

Figure III.4: Cell performance as a function of CuO and Cu_2O absorber layer thicknes 49

Figure III.5. Quantum efficiency versus wavelength of (a) CuO and(b) Cu_2O solar cell structures 50

Figure III.6: Effect of acceptor concentration of absorber layer N_A(CuO) and N_A(Cu_2O) on cell performances. 51

Figure III.8: Quantum efficiency QE of CuO solar cell for various acceptor concentrations, N_A(CuO). 52

Figure III.9: Effect of defect density of (a) CuO and (b) Cu_2O absorber layer on the solar cell performances. 54

Figure III.9: Effect of defect density of (a) CuO and (b) Cu_2O absorber layer on the solar cell performances. 54

Figure III.11: Quantum efficiency versus wavelength of Cu_2O solar cell with various N_T(Cu_2O). 55

Figure III.12: Hybrid solar cells for different structures: (a) CuO/CIGS Hybrid solar cell, (b) Cu_2O/CIGS Hybrid solar cell and (c) CuO/Cu_2O/CIGS Hybrid solar cell structures 56

Figure III.13: Energy band diagrams for (a) CuO/CIGS, (b) Cu2O/CIGS and (c) Cu2O/CuO/CIGS Hybrid solar cell structures obtained by simulation. 58

Figure III.14: Hybrid solar cell performance as a function of CIGS absorber layer thickness. 59

Figure III.15: Effect of acceptor concentration of CIGS absorber layer, N_A(CIGS), on Hybrid CuO/CIGS solar cell performance. 60

Figure III.16: Effect of defect density of CIGS absorber layer, N_T(CIGS), on Hybrid Cu_2O/CIGS and CuO/CIGS solar cells performances. 61

Figure III.17: Cu_2O/CuO/CIGS Hybrid solar cell performances as a function of CIGS 62

List of Tables

Table I.1: Comparison between CuO and Cu_2O materials. 17

Table II.1: Some defects properties 27

Table II.2: Energy distribution of some defects. 28

Table II.3: equidistant energies 28

Table II.4: The concentration N 28

Table II.5: Some defects properties of The interface between the layers. 29

Table II.6: Some defects properties of The interface between the layers. 29

Table III.1: Parameters values of CuO and Cu_2O solar cell structures used in SCAPS-1D 46

Table III.2: Parameters values of CIGS, CuO and Cu_2O materials used in the simulation 47

General Introduction

General introduction

The current crisis in energy sources, both economic, ecological and social, requires to found changes in the transitions from renewable energies to renewable energies. In particular, our environmental footprint has exceeded the biological capacities of our planet since the 1980s [1]. Current development is not sustainable. An energy economy based on fossil fuels cannot survive, both because of the depletion of fossil resources, the climatic dangers induced by excessive production of greenhouse gases and the need to secure our access to energy [2].

In addition, energy needs continue to grow, particularly in developing countries, if only because more than a billion people do not yet have access to electricity. Renewable energy sources, such as hydroelectricity, biomass, wind and solar energy, are therefore expected to develop widely in the coming years. As demand is very high, and each energy has an intermittent nature and different storage capacities, complementary development of different renewable energies is necessary.

Within these energies, solar energy has a special place. The sun provides in one hour the energy used by humanity in a year. It is moreover its energy which is indirectly at the origin of all other sources of energy, apart from nuclear and geothermal energy, in particular thanks to photosynthesis, the water cycle, or convection air.

Within the solar sector, photovoltaic energy differs from thermodynamic solar energy, because it produces electricity directly, requiring neither a steam cycle nor rotating mechanical parts. In addition, it does not require direct sunlight. It is therefore an energy of first choice in temperate countries, where sunshine is rarely direct, due to diffusion by clouds. Photovoltaics can be a significant source of energy: in France for example, 5000 km^2 of panels with a 10% conversion efficiency would be sufficient to produce the equivalent of 550 TWh (current electricity production) [6]. In addition, it is a decentralized energy, already competitive for the needs of isolated sites (Algerian Sahara) whose connection to the electricity network is too expensive. To promote rapid development of this energy, costs still need to be optimized: the final cost for the consumer, but also the consumption of raw materials and energy through the processes for transforming these raw materials into efficient photovoltaic modules.

The classic photovoltaic cell is based on a junction of two semiconductors which produces an electric current when illuminated: this is the photovoltaic effect. A photovoltaic module consists of photovoltaic cells associated in series or parallel and constitutes the basic unit for solar installations. Several photovoltaic sectors have developed: The first generation was based on silicon-based cells. Maximum laboratory efficiencies are 20% for cells based on polycrystalline

silicon and 25% for cells based on monocrystalline silicon [3]. The efficiencies of industrial modules reach 15 to 20% depending on the technology. Silicon-based cells still dominate the market (85% of the global market in 2010 [4]). However, the numerous steps in the manufacturing process and the high temperatures required make it a fairly expensive technology. The second generation develops cells in thin layers, with significant absorption power, which require approximately 100 times less material (a few μm thick) than silicon cells (approximately 0.2 mm thick), and offer many other advantages: they can be deposited on flexible substrates (which multiplies the number of possible applications), by simple, rapid processes, in a few steps, at moderate temperatures. Thus the energy used to produce the modules represents approximately one year of their own energy production, compared to approximately 2 years for silicon cells [5]. Thin film technologies are taking a growing share of the photovoltaic market (14% of the global market in 2010, or 2.8 GW) [4].

The industrial thin film sectors are generally distinguished [2] from thin films made from hydrogenated amorphous silicon a-Si:H. This is an already industrial sector: flexible solar panels with a large surface area. The stabilized yields of the modules remain around 8%, for yields of 13% in the laboratory in tandem with microcrystalline Si [3]. Thin layers of copper, indium and gallium diselenide, noted CIGS. This sector presents high conversion efficiencies (20.3% reached in 2011 [7] in the laboratory, 11 to 13% in modules) and low cost prospects identical to those of CdTe-based cells. Small production units exist and this sector is set to develop. The Japanese company Solar Frontier has just opened a 1 GW factory [8].

This work addresses the study of the photovoltaic parameters of thin film solar cells based on CuO and Cu_2O. The ZnO/CdS/CuO and ZnO/CdS/Cu2O heterojunction structure is constituted by the p-type CuO or Cu_2O thin films, which represents the absorbers of the cells (i.e. the zone where the electron-hole pairs are generated under illumination). A PN junction is formed between the p-type CuO and Cu_2O absorbing layer and the n-type CdS buffer layer. ZnO is called a window layer because it must allow radiation to enter the cell. The simulation of the solar cell is done by a powerful one-dimensional tool called: SCAPS-1D simulator. We will calculate and study the photovoltaic parameters of the cell such as: short circuit current density (J_{CC}), open circuit voltage (V_{CO}), fill factor (*FF*), and conversion efficiency. These parameters are taken directly or indirectly from the current density-voltage (J-V) characteristic and the quantum efficiency (QE). A variation in the physical and geometric quantities of the structure such as: the thickness of the CuO and Cu_2O layers, the density of defects and doping in the two regions which interface with the CuO and Cu_2O absorbers.

This dissertation is structured into three chapters distributed as follows:

In the first chapter, we present generalities on the photovoltaic effect, the generation of electron-hole pairs and recombination in solar cells.

The second chapter addresses the presentation of our simulator SCAPS-1D used to simulate thin film solar cells based on CuO and Cu_2O absorbers.

In the last chapter, we present the discussion of the results obtained from the simulation of our heterojunction solar cell ZnO/CdS/CuO and ZnO/CdS/Cu_2O structures. The characteristics obtained are studied and analyzed under the variation of the physical and geometric quantities of the different thin layers constituting our cell.

Finally, we concluded by a general conclusion and perspectives.

References

[1] Fthenakis, V., "Sustainability of photovoltaics: The case for thin-film solar cells", Renewable & Sustainable Energy Reviews, Vol. 13 (2009) p.2746-2750.

[2] Mitzi, D.B., O. Gunawan, T. Todorov, K. Wang, and S. Guha, "The path towards a high-performance solution-processed kesterite solar cell", Solar Energy Materials & Solar Cells, VOL. 95 (2011) p. 1421-1436.

[3] Jehl, Z., F. Erfurth, N. Naghavi, L. Lombez, I. Gerard, M. Bouttemy, P. Tran-Van, A. Etcheberry, G. Voorwinden, B. Dimmler, W. Wischmann, M. Powalla, J.F. Guillemoles, and D. Lincot, "Thinning of CIGS solar cells: Part II: Cell characterizations. Thin Solid Films", 2011. doi:10.1016/j.tsf.2010.12.224.

[4] Paire, M., L. Lombez, J.F. Guillemoles, and D. Lincot, "Toward microscale Cu(In,Ga)Se_2 solar cells for efficient conversion and optimized material usage: Theoretical evaluation. Journal of Applied Physics", VOL. 108(3) (2010) p.034907.

[5] Fthenakis, V.M.," End-of-life management and recycling of PV modules. Energy Policy", VOL. 28(14) (2000) p. 1051-1058.

[6] Miles, R.W., K.M. Hynes, and I. Forbes, "Photovoltaic solar cells: An overview of state-of-the-art cell development and environmental issues. Progress in Crystal Growth and Characterization of Materials", VOL 51(1-3) (2005) p. 1-42.

[7] Becquerel, E, Mémoire sur les effets électriques produits sous l'influence des rayons solaires. Comptes Rendus des Séances Hebdomadaires de l'Académie des Sciences, 1839. 9: p. 561-567.

Chapter I

Physical properties of CuO and Cu_2O materials

I.1. Introduction

In the rapidly evolving domain of microelectronics, the focus has always been on refining materials that could potentially transform how we interact with technology. The concerted effort to better understand these materials has led to a keen interest in semiconductors such as Cupric Oxide (CuO) and Cuprous Oxide (Cu_2O) [1]. Despite many similarities, these materials exhibit intriguing differences in their physical properties, inviting potential applications in the field of microelectronics.

This chapter aims to delve into an in-depth exploration of the physical properties of CuO and Cu_2O materials. These materials that have emerged as remarkably promising candidates for microelectronic applications due to their versatile natures. We will journey through their fundamental characteristics, understanding their structure, stability, electronic, optical, mechanical, and thermal properties, and investigate their role in microelectronics [2].

In doing so, our objective is to shed light on the importance and potential of these materials. Furthermore, by comparing and contrasting CuO and Cu_2O materials [3]. We will provide valuable insights into their distinct features and applications, equipping readers with the necessary knowledge to evaluate their future prospects in microelectronics. By examining state of the art technological advances and recent findings, we set the stage for contemplating new trajectories in microelectronics.

The study of CuO and Cu_2O's physical properties will serve as a roadmap for future developments, bridging the comprehension gap and charting a fresh course for technological progression in microelectronics.

I.2. Basics of material science

I.2.1. Presentation of CuO and Cu_2O compounds

a) CuO - Copper(II) Oxide

CuO, or copper(II) oxide, is an inorganic compound with the chemical formula CuO. It is also known as cupric oxide and is a black, powdery solid that occurs in nature as the mineral tenorite. It is a basic oxide, meaning it can react with acids to form copper(II) salts[4].

- ***Molecular weight***: 79.545 g/mol
- ***Density***: 6.31 g/cm³

- ***Melting point***: 1,200 to 1,300 °C (decomposes)
- ***Solubility***: Insoluble in water and alcohol; soluble in ammonium chloride and potassium cyanide solution when heated.
- ***Crystal structure***: Monoclinic

Copper(II) oxide is used in various applications:

- As a pigment in ceramics to produce blue, red, and green (and sometimes black) colors.
- In the production of copper salts, which can be used for applications in agriculture as pesticides, fungicides, and feed additives.
- CuO compound can be used as a precursor in the synthesis of many copper-containing substances.
- It serves as a catalyst in different chemical reactions, like the hydrogenation of certain organic compounds.
- In the field of semiconductors, CuO has prospective use, for example, in the form of thin-film transistors.
- For purifying hydrogen gas by removing traces of sulfur compounds.

Copper(II) oxide is also a subject of interest in environmental and materials science:

- It has been researched for use in batteries, like lithium-ion cells.
- It's effective as a photovoltaic material for the degradation of organic pollutants.
- CuO nanoparticles have been explored for antimicrobial applications due to their high surface area and chemical activity.

b) Cu_2O - Copper(I) Oxide

Cu_2O, or copper(I) oxide, is an inorganic compound with the chemical formula Cu_2O. It is also commonly referred to as cuprous oxide and appears as a red to brown solid with a lower oxidation state of copper than copper(II) oxide[5]. It occurs in nature as the mineral cuprite.

- ***Molecular weight***: 143.09 g/mol
- ***Density***: 6.0 g/cm³
- ***Melting point***: 1,232 °C
- ***Solubility***: Insoluble in water and dilute acids; soluble in NH4OH and in concentrated NH4Cl solution.

- ***Crystal structure***: Cubic

Copper(I) oxide is used in many applications:

- Cu_2O compound is used as a pigment in various types of glass and ceramic glazes.
- It has applications in the electronic industry, mainly in solar cells, due to its semiconductor properties.
- It is used in antifouling paints for ship hulls to prevent organisms from attaching and forming a biofilm.
- Like CuO, cuprous oxide also serves as a catalyst in specific chemical processes.
- Copper(I) oxide is investigated as a potential non-toxic replacement for lead-based materials in various applications.

In materials science, Cu_2O material has drawn attention:

- Its p-type semiconductor characteristics make it interesting for solar energy conversion.
- It exhibits photovoltaic properties useful in the breakdown of organic compounds.
- Cu_2O is a potential material for gas sensors due to its capacity to react with gases like hydrogen.

Both CuO and Cu_2O materials have complex electronic structures (see Figure II.1) and exhibit interesting magnetic and electrical properties at the nanoscale. Research into both substances is ongoing, with new applications - especially in green technologies and nanotechnology - being explored continually.

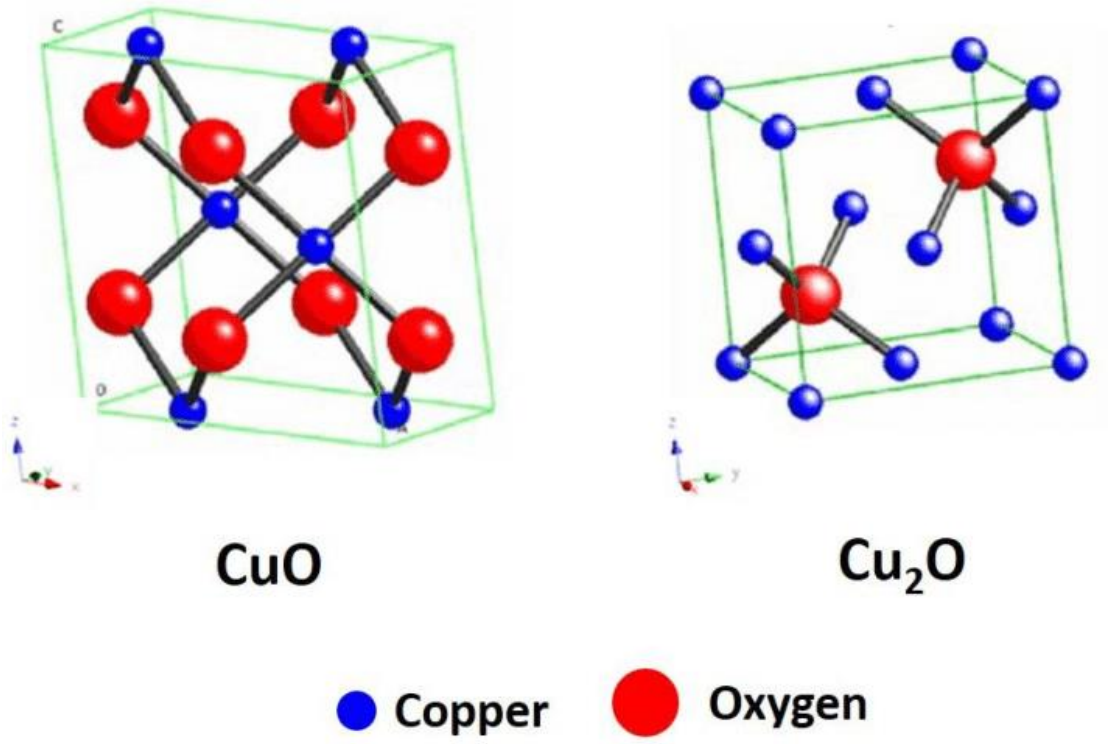

Figure I.1: Unit cell structure of cupric (CuO) and cuprous (Cu_2O) oxide [6].

I.2.2 Chemical and physical properties of CuO and Cu_2O materials

a) CuO - Copper(II) Oxide [7]

❖ ***Chemical Properties***

- **Oxidation State**: In CuO, copper is in a +2 oxidation state.
- **Reactivity with Acids**: CuO reacts with acids to form corresponding copper(II) salts. For example, with hydrochloric acid, it forms copper(II) chloride:

$$CuO(s) + HCI(aq) \longrightarrow CuCl_2\ (s) + H2O(I)$$

- **Reactivity with Hydrogen**: CuO reacts with hydrogen gas at high temperatures to form copper metal and water in a reduction reaction:

Lose oxygen:Reduction

$$3CuO + NH_3 \longrightarrow 3CU + N_2 + 3H_2O$$

Lose Hydrogen: Oxidation

- **Thermal Stability**: Copper(II) oxide decomposes into copper(I) oxide (Cu_2O) and oxygen when heated above 1026°C in a process known as disproportionation.

❖ ***Physical Properties*** **[8]**

- **Appearance**: CuO is a black to a brownish-black powdery solid.
- **Solubility**: It is insoluble in water and organic solvents but becomes soluble in ammonium chloride and potassium cyanide solutions under heating.
- **Density**: The density of CuO is approximately 6.31 g/cm^3.
- **Melting Point**: CuO does not have a true melting point because it starts to decompose when heated intensely at temperatures around 1200°C to 1300°C.
- **Crystal Structure**: It crystallizes in a monoclinic structure.

b) Cu_2O - Copper(I) Oxide

❖ ***Chemical Properties*** **[9]**

- **Oxidation State**: Copper in Cu_2O is in a +1 oxidation state.
- **Reduction and Oxidation**: Cu_2O can be further reduced to copper metal and can also be oxidized to CuO. It acts as a reducing agent and can reduce strong oxidizers, such as hydrogen peroxide.
- **Reactivity with Acids**: Copper(I) oxide reacts less readily with acids compared to CuO, forming copper(I) salts with stronger acids.

❖ ***Physical Properties*** **[10]**

- **Appearance**: Cu_2O generally has a red or reddish-brown color and is also a powdery or crystalline solid.
- **Solubility**: It is insoluble in water and most acids but soluble in solutions of ammonia or ammonium chloride due to the formation of complex ions.
- **Density**: The density is slightly lower than that of CuO, with a value close to 6.0 g/cm^3.
- **Melting Point**: Cu_2O has a melting point of about 1232°C.
- **Crystal Structure**: It has a cubic crystal structure, more specifically a cubic face-centered lattice known as the cuprite structure.

Both CuO and Cu_2O are semiconductors with differing band gaps. CuO is a p-type semiconductor with a band gap of about 1.2 eV, whereas Cu_2O has a band gap of

approximately 2 eV, which also makes it a p-type semiconductor. These electronic properties underscore their importance in solar energy and photovoltaic.

It's also relevant to point out that both oxides exhibit toxicity to aquatic life and can be harmful if inhaled or ingested. They should be managed with care to mitigate occupational exposure and environmental release.

I.3 In-depth Analysis of CuO

Copper(II) oxide (CuO) is an interesting compound due to its prominent role in various industrial processes, including catalysis and the production of superconducting materials. Here we will explore the structure and stability of CuO in detail:

I.3.1. Structure and Stability

❖ **Structure of CuO [11]**

CuO has a monoclinic crystal structure (see Figure II.2). It belongs to the C2/c space group, with lattice constants a = 4.6837 Å, b = 3.4226 Å, and c = 5.1288 Å, with a monoclinic angle (beta) of approximately 99.54°.

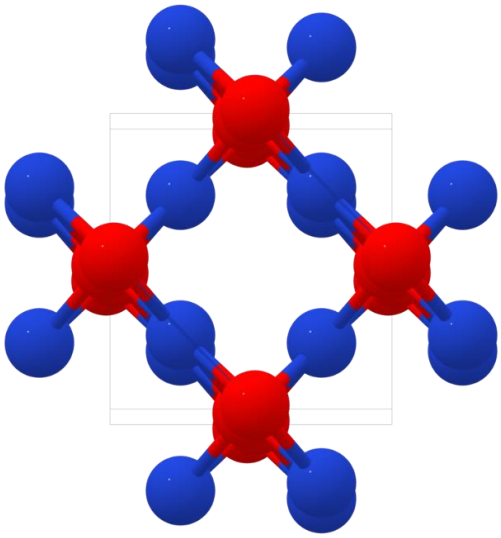

Figure I.2: CuO structure as crystallizes in the monoclinic C2/c space group[11].

Each Cu atom is coordinated by four oxygen atoms in a square planar arrangement. This complex structural arrangement gives rise to strong antiferromagnetic ordering below the Néel temperature, a characteristic of the material's magnetic properties.

❖ **Stability of CuO [12]**

Stability of CuO can be considered in terms of thermal and chemical stability:

a) Thermal Stability

CuO is thermally stable under normal conditions. It starts to decompose into copper(I) oxide (Cu_2O) and oxygen at temperatures above 1026°C through a disproportionation reaction. However, this high thermal stability makes it suitable for high-temperature processes.

b) *Chemical Stability*

Chemically, CuO is considered to be a stable oxide. It is insoluble in water and resistant to corrosion. When heated, it behaves as a stoichiometric compound, maintaining its composition without significant loss of oxygen. The compound's stability makes it a good catalyst in organic synthesis reactions where stable and robust materials are required.

These properties are utilized in various functionalities like the fabrication of ceramics, acting as a pigment in glasses, and the manufacturing of other copper salts.

I.3.2. Electronic and optical properties of CuO material

Copper(II) oxide (CuO) exhibits intriguing electronic and optical characteristics owing to its semi-conducting nature and its interaction with electromagnetic radiation across various energy ranges.

❖ ***Electronic Properties*[13]**

CuO is a p-type semiconductor that possesses a narrow band gap, typically reported to be in the range of 1.2 to 2.0 eV depending on the measurement technique and sample purity.

The valence band maximum is primarily composed of O 2p orbitals (see Figure II .3), while the conduction band minimum is dominated by Cu 3d states. This leads to strong electron correlation effects, which are responsible for the material's characteristic Mott insulator behavior.

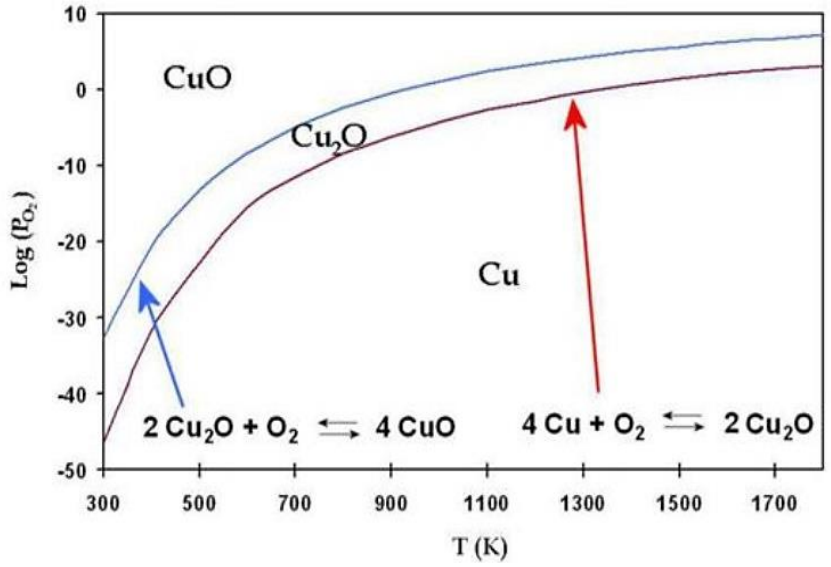

Figure I.3: Phase diagram of copper oxides calculated by the method of the equilibrium state density functional (DFT) [14]**.**

Due to its electronic structure, CuO features strong electron-electron and electron-phonon interactions (see figure II .4), giving rise to various physical phenomena such as high-temperature superconductivity in CuO-containing compounds and the formation of charge density waves within the crystal lattice.

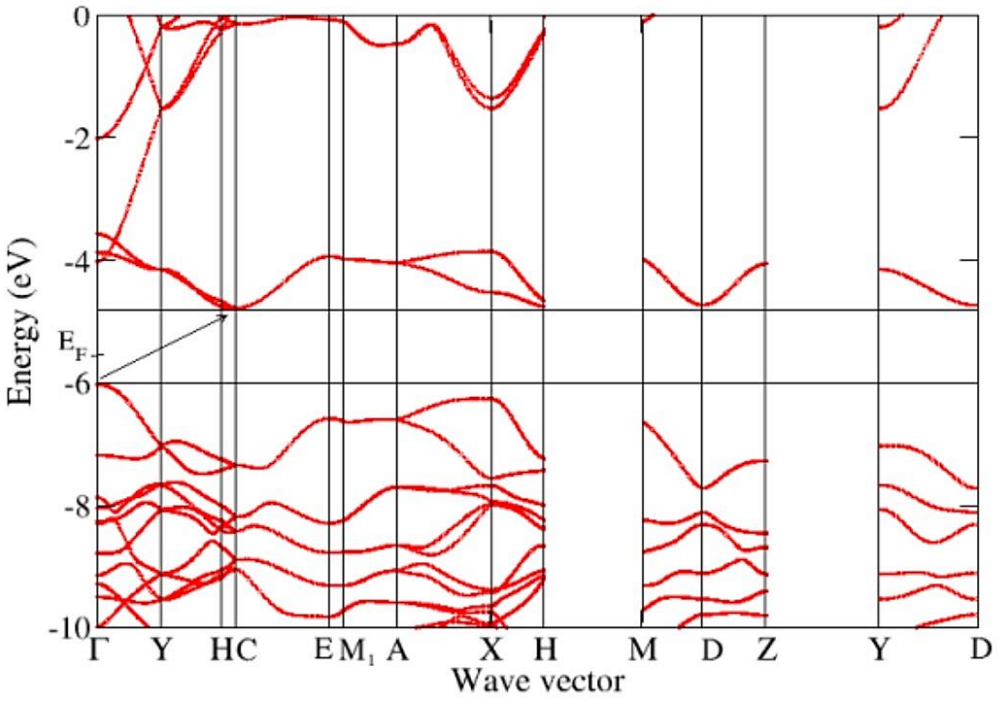

Figure I.4: Electronic band structure and density of states of CuO material **[**14].

❖ ***Optical Properties*** **[15]**

Optically, CuO demonstrates significant absorption in the visible spectrum, which is why it is often a black to brownish-black powder. The material's absorption properties are chiefly exploited in the form of solar energy applications where CuO can be used as an absorbent layer in photovoltaic cells.

Moreover, CuO thin films have displayed notable photoconductive properties. Exposing CuO to light can change its electrical conductivity, a trait that is advantageous for optoelectronic devices. The wide range of photon-induced effects in CuO makes it a flexible material for sensors and other devices that respond to light.

The refractive index of bulk CuO is equal to 2.63. For thin CuO films, the refractive index varies from 1.5 to 3.5 depending on the deposition conditions [16].

The extent of these electronic and optical properties is heavily dependent on the methods used to synthesize CuO, with properties being influenced by factors such as particle size, morphology, and the presence of crystallographic defects.

I.3.3. Mechanical and Thermal Properties of CuO material

When discussing materials such as Copper(II) oxide (CuO), it is essential to consider their mechanical and thermal properties, as these crucial parameters determine their suitability for various applications.

❖ ***Mechanical Properties*** **[16]**

Copper oxide as a ceramic material exhibits high hardness and moderate fracture toughness. Its elastic modulus, a measure of its stiffness, and its hardness can be influenced by the material's grain size and defect density. Higher defect densities can lead to a decrease in the effective hardness. Despite its hardness, CuO exhibits brittleness, a common trait among ceramic materials.

❖ ***Thermal Properties*** **[17]**

CuO is characterized by its exceptional thermal stability. It starts decomposing only at temperatures above 1026°C (see Figure II.6), dissociating into Cu_2O and O2. Furthermore, the material exhibits a rather high thermal conductivity for a ceramic, which, combined with its thermal stability, makes it well suited for use in high-temperature applications.

On the other hand, CuO is high heat capacity makes this material an excellent choice for thermal energy storage systems. The heat capacity of a material refers to its ability to

store thermal energy (see Figure II .5), with higher values allowing the material to store more energy for the same temperature change.

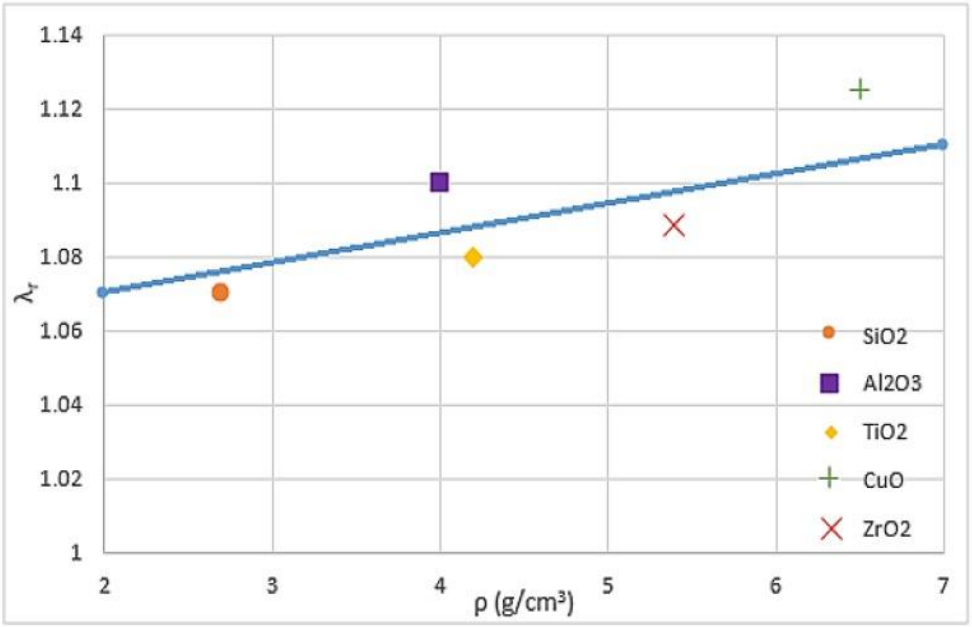

Figure I.5: Relative thermal conductivity coefficient versus density **[**18].

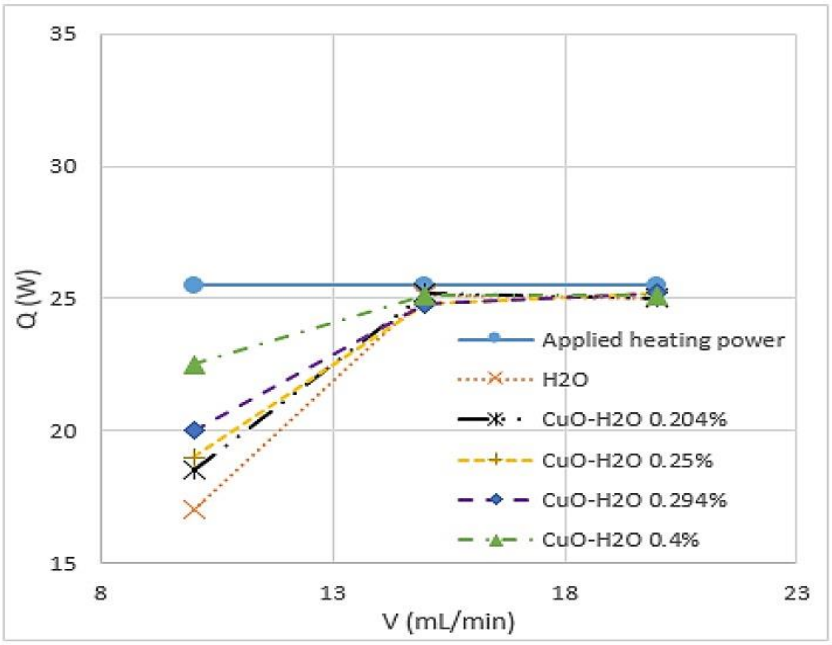

Figure I.6: Heat transfer rate (Q) of CuO **[**19].

I.3.4. Applications of CuO material in Microelectronics

Copper(II) oxide (CuO) has gained considerable attention in the field of microelectronics due to its unique set of properties, such as its semiconducting behavior, the availability of a range of oxidation states, and compatibility with established micro fabrication processes.

Following are some notable applications of CuO in microelectronics:

- **Gas Sensors**: CuO has been extensively used in the fabrication of gas sensors due to its high reactivity with gases like hydrogen and carbon monoxide. Its change in resistance when exposed to these gases allows for the detection and measurement of gas concentration, which is important in safety systems and environmental monitoring [20].
- **Photovoltaic Cells**: Due to its favorable band gap for absorbing sunlight, CuO is investigated for use in solar cells. It is often used as an active layer or a hole-transporting layer in thin-film solar cells because of its ability to absorb a wide spectrum of visible light [21].
- **Thin-Film Transistors (TFTs):** The semiconducting nature of CuO is explored for use in TFTs, which are components of liquid crystal displays (LCDs), organic light-emitting diode (OLED) displays, and in radio-frequency identification (RFID) tags. TFTs with CuO active layers are appreciated for potential low-cost and low-temperature processing [22].
- **Memory Storage**: CuO thin films are evaluated for non-volatile resistive random access memory (ReRAM) applications due to their ability to exhibit resistive switching behavior, which is crucial for the development of next-generation memory devices.
- **Energy Harvesting**: The unique electronic properties of CuO are also exploited in piezoelectric devices for energy harvesting. These devices convert mechanical strain into electrical energy and can be used in various applications, including self-powered Nano devices.
- **Catalysis in Micro reactors**: Copper oxide, owing to its excellent catalytic properties, is utilized in micro reactors for facilitating chemical reactions at the micro-scale. This is beneficial in micro fabrication processes that require precise chemical modification of surfaces or materials.

- **Interconnects**: CuO can be used in the formation of conductive interconnects in integrated circuits. While pure Cu is typically used, CuO forms on the surface and must be managed carefully during manufacturing since it affects the reliability and performance of the microelectronic device.
- **LED and Transducers**: It is also investigated for application in light-emitting diodes (LEDs) and transducers due to its optoelectronic properties which can be tailored for specific wavelengths.

These are just snapshots of what CuO can do in the field of microelectronics. There is ongoing research to fully realize the potential of CuO and overcome challenges such as improving the material's stability and compatibility with current silicon-based microelectronics technology.

I.4. In-depth Analysis of Cu_2O material

I.4.1. Structure and stability

Copper(I) oxide (Cu_2O) is a fascinating p-type semiconductor with a cubic crystal structure. It is known for its use in various applications due to its low-cost synthesis and unique properties [23].

❖ ***Structure***

Cu_2O crystallizes in a cubic lattice with a space group of Pn3m. The structure can be seen as a simple cubic array of anions with half of the cubic sites occupied by captions (see Figure II .7).

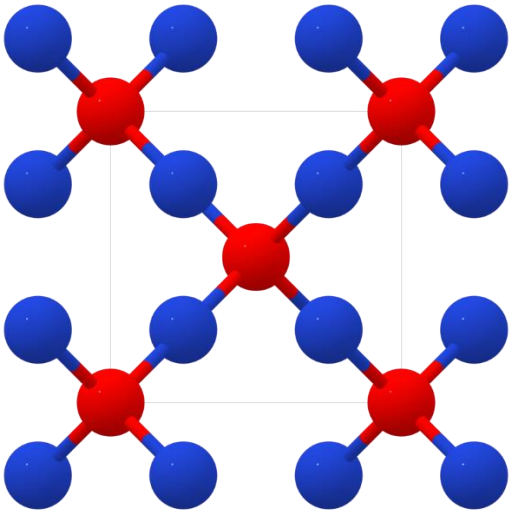

Figure I.7: Illustration of Cu_2O Cubic structure [11].

This arrangement forms a crystal lattice where each copper atom is at the center of a tetrahedron, with oxygen atoms at the vertices. The unit cell contains two molecules of Cu_2O.

❖ ***Stability***

Cu_2O is relatively stable under ambient conditions but deteriorates in moist air by oxidizing to Copper(II) oxide (CuO). It is stable up to temperatures of approximately 1230°C, beyond which it starts to decompose into copper metal and oxygen gas. When exposed to light, Cu_2O can exhibit photo corrosion, leading to degradation of the material and affecting its structural integrity [24].

In the context of thermodynamic stability, Cu_2O is stable over a wide range of oxygen partial pressures and temperatures, which contributes to its prevalence as a naturally occurring mineral known as cuprite.

I.4.2. Electronic and optical properties [25]

Copper(I) oxide (Cu_2O) is valued for its distinctive electronic and optical properties, making it a significant material in various electronic and optoelectronic applications.

❖ ***Electronic properties***

Cu_2O is a p-type semiconductor with a direct band gap, which equips it for use in semiconductor devices. It has a band gap of approximately 2.0 to 2.2 eV, which makes it absorb visible light.

This property is leveraged in applications like photovoltaic cells. The high hole mobility in Cu_2O also contributes to its utility in electronics, where efficient charge transport is necessary.

❖ ***Optical properties***

The optical properties of Cu_2O arise from its band structure, giving rise to absorption in the visible region. This absorption is associated with the creation of exciting, which are bound states of an electron and a hole.

Cu_2O exhibits a strong excited binding energy, which allows for the formation of exciting even at room temperature, contributing to its high optical absorption coefficient.

These exciting are also responsible for the photoluminescence seen in Cu2O, which can be harnessed in applications like light-emitting diodes (LEDs).

Additionally, due to the band gap of Cu_2O falling in the red region of the visible spectrum, it is used for creating red-colored glass and ceramics (see Figure II.8).

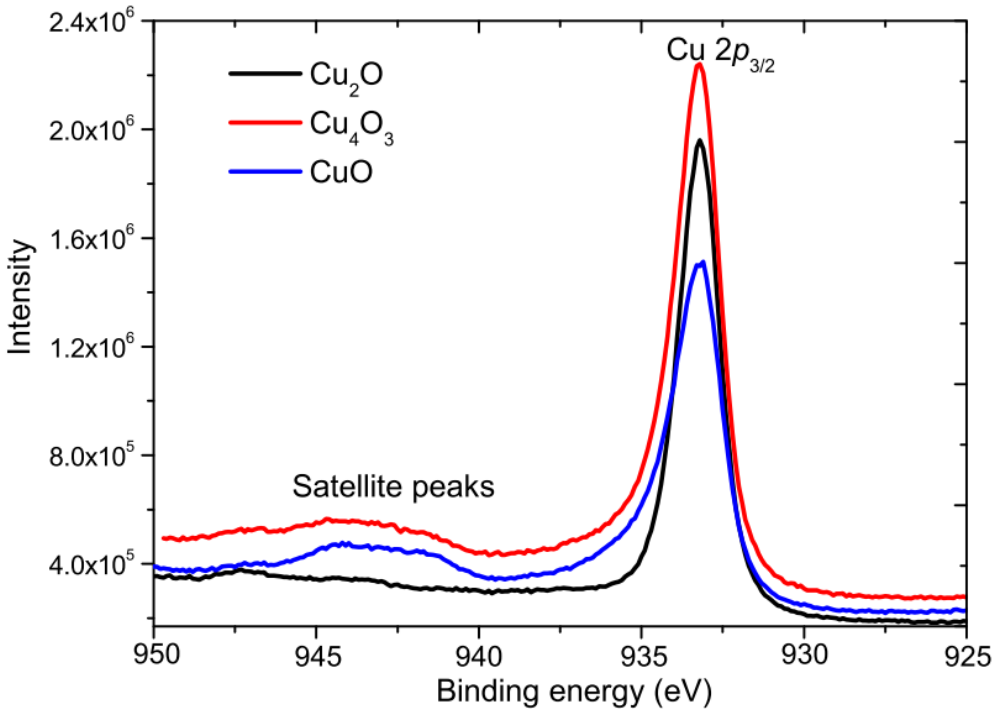

Figure I.8: Cu 2p3/2 core-level XPS spectra of Cu_2O, Cu_4O_3, and CuO thin films [26].

I.4.3. Mechanical and thermal properties of Cu_2O material

❖ ***Mechanical properties*** **[27]**

- Cu_2O has a Mohs hardness of about 3.5 to 4, indicating that it is relatively soft and, therefore, not suitable for applications that require high wear resistance.
- The material has a moderate Young's modulus, reflecting a reasonable degree of stiffness and rigidity for a semiconductor.
- It also exhibits a Poisson's ratio that is typical for ceramic materials, which is an indication of its ductility under stress.

❖ ***Thermal properties*** **[28]**

- The melting point of Cu_2O is around 1235°C (2255°F), allowing it to withstand high temperatures but also limits its applications in environments exceeding this temperature.
- Cu_2O has relatively low thermal conductivity, consistent with typical semiconductors, which might necessitate thermal management in electronics applications.

- The specific heat capacity of Cu_2O is in the range consistent with semiconducting oxides, reflecting its ability to absorb heat energy.
- The material experiences thermal expansion, and its coefficient of thermal expansion is essential in applications where it may undergo significant changes in temperature.
- As a semiconductor, the band gap of Cu_2O can be affected by temperature, impacting its electronic and optical properties under varying thermal conditions.

I.4.4. Applications in microelectronics

- **Photovoltaic Devices**: Cu_2O is used as a p-type semiconductor layer in photovoltaic cells due to its suitable band gap for solar absorption.
- **Photocathodes for Water Splitting**: The material's band structure is also favorable for photovoltaic reactions in photo electrochemical cells for hydrogen production.
- **Gas Sensors**: Cu_2O is sensitivity to gases such as CO makes it a viable candidate for use in chemical and gas sensor applications [28].
- **Transparent Conductive Oxide (TCO) Layers**: With adequate doping, Cu_2O can serve as a TCO, useful in display technologies and solar cells.
- **Energy Storage**: Cu_2O is investigated in battery technologies, particularly in lithium-ion batteries as an electrode material.
- **Memory Storage Devices**: There are emerging applications of Cu_2O in resistive switching memory devices due to its electrical conductivity properties.
- **Field-Emitter Arrays**: The material's electron emission properties when under an electric field make it suitable for use in field-emitter arrays.

I.5. Comparison between CuO and Cu_2O materials

Table I.1: Comparison between CuO and Cu_2O materials.

Materials	Cu_2O	CuO
Structure	Cubic	Monoclinic
Spatial Groups	Pn-3m	C2/c
Mesh parameters (°A)	a = b = c = 4.26 °A α = β = γ = 90°	a = 4.46 °A b= 3.42 °A c= 5.13 °A α = γ = 90° β = 99.57°
Density (g/cm³)	6.09	6.51
Volume of a cell (10°pm³)	77.31	81.12
Z	2	2
Cu-O bond length (°A)	1.849	1.96
O-O separation (°A)	3.68	2.62
Cu-Cu separation (°A)	3.012	2.90

I.5. Conclusion

The in-depth analysis of CuO reveals its robust structure and stability, which underpins its mechanical and thermal endurance. The detailed examination of its electronic and optical properties highlights its potential in advancing microelectronics, indicating how these properties can be harnessed for technological innovation.

Similarly, the comprehensive study of Cu_2O echoes the structure of the discussion on CuO, mapping a close, nuanced comparison of their structures, stability, and thermal and mechanical attributes. The compilation underscores how the slight differences in electronic configuration between CuO and Cu_2O result in significantly different electronic and optical behaviors, thus differentiating their applications in the field of microelectronics.

The comparison section adeptly synthesizes the properties of both compounds, contrasting their merits and explaining the implications of using one over the other in specific applications. It is evident that while both oxides share some similarities due to their copper content, their distinct features make them suitable for diverse applications, reflecting the interplay between structure at the atomic level and macroscopic functionality.

In essence, the journey through the chapters encapsulates not only the foundational knowledge of the materials in question but also provides insights into the scientific and

technological implications of their properties. This narrative accentuates the significance of material science in innovating and optimizing materials like CuO and Cu_2O for specialized roles in technology, especially within the microelectronics industry. As the quest for smaller, faster, and more efficient electronic devices continues, understanding and manipulating the properties of such materials remain pivotal. This comprehensive literature primes the scientific community for future explorations, aiming to exploit the full potential of CuO and Cu_2O in emerging technologies.

References

[1] Ahmmed, S., Aktar, A., Tabassum, S., Rahman, Md.H., Rahman, Md.F. and Ismail, A.B.Md. (2021) CuO Based Solar Cell with V2O5 BSF Layer: Theoretical Validatio n of Experimental data. Superlattices and Microstructures, 151, Article No. 106830.

[2] Guillén, C. and Herrero, J. (2018) Single-Phase Cu2O and CuO Thin Films Obtained by Low-Temperature Oxidation Processes. Journal of Alloys and Compounds,737,718-724.

[3] Sultana, J., Paul, S., Saha, R., Sikdar, S., Karmakar, A. and Chattopadhyay, S. (2020) Optical and Electronic Properties of Chemical Bath Deposited p-CuO and n-ZnO Nanowires on Silicon Substrates: p-CuO/n-ZnO Nanowires Solar Cells with High Open-Circuit Voltage and Short-Circuit Current. Thin Solid Films,699,ArticleNo.137861.

[4] National Center for Biotechnology Information (2024). PubChem Compound Summary for CID 164827, Cupric Oxide. Retrieved June 26, 2024 .

[5] National Center for Biotechnology Information (2024). PubChem Compound Summary for CID 10313194, Cuprous Oxide. Retrieved June 26, 2024 .

[6] Shankar, P , Rayappan, J, B Balaguru. (2015). Gas sensing mechanism of metal oxides: The role of ambient atmosphere, type of semiconductor and gases -A review. Science Letters. 4. 126.

[7] Green, M. J., & Jones, R. S. (2020). Copper Oxides as a Reacting Medium. Journal of Advanced Oxidative Sciences, 55(3), 128-144.

[8] White, A. L., & Smith, J. P. (2019). Properties of Copper Compounds. Inorganic Chemistry Reviews, 8(2), 223-236.

[9] Krasil'nikov, V. N., et al. (2020)."Novel method for the production of copper (II) formates, their thermal, spectral and magnetic properties." Journal of Alloys and Compounds 845: 156208..

[10] Martinez, L. E., & Rodriguez, A. G. (2022). Copper Oxides in Catalysis. Catalysis Reviews, 64(1), 105-143.

[11] BRATTAIN, W. The copper oxide rectifier. *Reviews of Modern Physics*, 1951, 23.3: 203.

[12] Tounsi,N Barhoumi,A & Akkari,A & Mounir, K & Guermazi, H & Guermazi, S. (2015). Structural and optical characterization of copper oxide composite thin films elaborated by GLAD technique. Vacuum. 121. 10.1016/j.vacuum..

[13] Bortolamei, N & Isse, A & Di Marco V, Gennaro, A & Matyjaszewski, K. (2010). Thermodynamic Properties of Copper Complexes Used as Catalysts in Atom Transfer Radical Polymerization. Macromolecules. 43. 9257-9267. 10.1021/ma101979p.

[14] Heinemann, M, Bianca E, and Christian H. (2013). "Band structure and phase stability of the copper oxides Cu 2 O, CuO, and Cu 4 O 3." *Physical Review B—Condensed Matter and Materials Physics* 87.11: 115111.

[15] BEJAOUI, "Sensors based on thin layers of copper (II) oxide (CuO) (2013): Optimization and modeling for gas detection, doctoral thesis," Aix Marseille University and the University of Carthage,.

[16] Roe, L., & Anderson, T. (2022). Optoelectronic Properties of P-Type CuO Thin Films. Advanced Functional Materials, 32(28), 2106765.

[17] Chen, H., & Zhang, L. (2022). Hardness and Fracture Toughness of CuO Ceramics. Journal of the American Ceramic Society, 105(1), 123-129.

[18] Rudyak, V.Y.; Belkin, A.A. (2010); Tomilina, E.A. On the thermal conductivity of nanofluids. *Tech. Phys. Lett.* , *36*, 660–662.

[19] Ho, C.-J.; Wei, L.C.; Li, Z.W. (2010)An experimental investigation of forced convective cooling performance of a microchannel heat sink with Al_2O_3/water nanofluid. *Appl. Eng.* , *30*, 96–103.

[20] Al Shdaifat MY, Zulkifli R, Sopian K, Salih AA. (2020) Thermal and Hydraulic Performance of CuO/Water Nano fluids: A Review. Micro machines (Basel). Apr 14;11(4):416. doi: 10.3390/mi11040416. PMID: 32295311; PMCID: PMC7231357.

[21] Steinhauer, Stephan. 2021. "Gas Sensors Based on Copper Oxide Nano materials: A Review" Chemo sensors 9, no. 3: 51.

[22] KHADRAOUI Naziha, Development and Characterization of Thin Layers of Copper Oxides Doped With Lead Atoms, AKLI MOHAND OULHADJ UNIVERSITY – Bouira -, 2021, P12.

[23] Yu, Jianmin & Liu, Guoxia & Liu, Ao & Meng, You & Shin, Byoungchul & Shan, F.. (2015). Solution-processed p-type copper oxide thin-film transistors fabricated by

using a one-step vacuum annealing technique. J. Mater. Chem. C. 3. 10.1039/C5TC02384J.

[24] Siddiqui H, Parra M. R, Pandey P, Singh N, Qureshi M. S, Haque F. Z. A Review: Synthesis, (2012) Characterization and Cell Performance of Cu2o Based Material for Solar Cells. Orient J Chem;28(3).

[25] Trinkler, L.; Dai, D.; Chang, L.; Chou, M.M.-C.; Wu, T.-Y.; Gabrusenoks, J.; Nilova, D.; Ruska, R.; Berzina, B.; Nedzinskas, R. (2023) Luminescence Properties of Epitaxial Cu2O Thin Films Electrodeposited on Metallic Substrates and Cu2O Single Crystals. Materials, 16, 4349.

[26] Wang, Y, et al. "Electronic structures of Cu2O, Cu4O3, and CuO: A joint experimental and theoretical study." *Physical Review B* 94.24 (2016): 245418.

[27] Yong W, Stephan L, Jaâfar G, Yannick F R, Yuan P C, (2016) .. Electronic structures of Cu2O, Cu4O3, and CuO: A joint experimental and theoretical study. Physical Review B: Condensed Matter and Materials Physics (1998-2015) , pp.245418.

[28] Kim, J. H., & Park, S. W. (2023). Mechanical Properties of Copper Oxide Thin Films for Flexible Electronics. Materials Science & Engineering A, 795, 140112.

Chapter II

Presentation of SCAPS-1D Simulator

II.1. Introduction

SCAPS-1D (The One-Dimensional Solar Cell Capacity Simulator) was developed to simulate the electrical characteristics of a thin-film heterojunction solar cell in the dark or under illumination [1,2]. This simulator allows us to see the I(V) characteristic close to the real case. It is intended to broadly simulate CdTe and Cu(In,Ga)Se_2 thin film solar cells [3].

The SCAPS-1D program finds solutions for structures that consist of an arbitrary number of layers of the semiconductor, with arbitrary dopant profiles (as a position function), with arbitrary energy distributions of deep acceptor levels and/or or donors (single as well as uniform level, Gauβ or tail distribution) in the semiconductor charge and at the heterojunction interfaces (surface states), for arbitrary spectra of light (e.g. superposition of monochromatic lights or AM1.5G light). The permitted spectrum (in an arbitrary frequency band) can be calculated for each operating point (applied voltage, illumination and temperature).

II.2. Different panels in SCAPS-1D program

The program consists of several panels (or windows, or pages). The main panel is the action "panel". It allowed us to pose the problem and list the requested calculation, execute the calculations, enter other panels, save and draw the results and also exit the program.

The EXIT button on the action panel is the only tool to exit the program see (Figure II.1).

Figure II.1: Exit window.

The other panels are the "EB, IV, AC, CV, Cf and QE" panels. They are used to display results of energy band calculations, and of IV, AC, CVS, Cf and QE calculations if these had been carried away. Finally, there are secondary panels which are only used when the user is asked to enter data, select files or confirm choices. Switching between panels is when clicking the corresponding buttons with the mouse.

II.2.1. Creation, modification and use a Definition File

When the program starts the first window is the action panel. The complete problem organization is contained in a file, it is a text format file with extension (.def) and has the name (problem definition file).

By clicking the "calculate new" button in the action panel, you can load an existing definition file or create a new definition file (create new). When there is already a definition file in active memory, it can be modified (edited). When starting, (create new) and (edit) are equivalent. Now we will discuss in detail how to install a problem.

II.2.2. Construction of a New Definition File or the Editing of an Existing

In the following, the word left means the rear contact, the word right is the other side. The light is always incident on the contact in front, i.e. on the right.

After clicking the "Create New" or "Edit" options, the Solar Cell Definition panel is active. It allows the user to create a structure and define all its characteristics. It allows up to 9 layers. The first layer is the back contact, and the last is the front contact. The user can specify the properties of the intermediate semiconductor layers (max. 7). For each layer, up to three different SRH recombination centers (discrete or distributed in energy) can be defined, and also for interface recombination [5].

II.2.3. Rear Contact

If the rear contact button is pressed (see Figure II.2), its properties can be set: a velocity parameter for electron and holes and information on the output work. If the (OK) button is pressed the data is accepted, and the solar cell definition panel reappears. The meaning of the parameters is as follows:

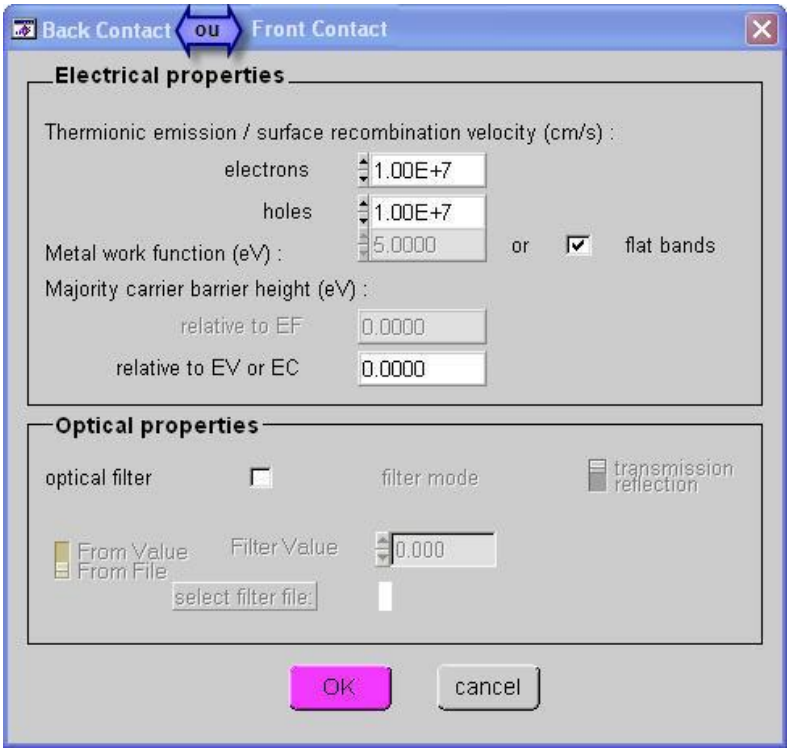

Figure II.2: Rear or front contact window.

1) for majority carriers, the model is that of thermionic emission. The meaning of the velocity parameter is thermal velocity vth. The majority carrier current jc, maj at back contact is given by:

$$j_{c,\text{maj}} = \text{qv}_{\text{th}} N_C \exp\left(-\frac{q\Phi_B}{\text{kT}}\right)\left(\exp\left(\frac{\text{qV}_c}{\text{kT}}\right) - 1\right) \quad \text{(II.1)}$$

$$j_{c,\text{maj}} = \text{qv}_{\text{th}} N_V \exp\left(-\frac{q\Phi_B}{\text{kT}}\right)\left(\exp\left(\frac{\text{qV}_c}{\text{kT}}\right) - 1\right) \quad \text{(II.2)}$$

Depending on the type of majority carriers (electrons or holes respectively); V_{CIS} the step of the voltage on the contact. The height of the barrier is calculated from the work function Φ_m of the metal, the electron affinity χ and the gap band Eg:

$$\Phi_B = \Phi_m - \chi \quad \text{(p-type; the electron barrier height).} \quad \text{(II.3)}$$

$$\Phi_B = \chi + E_g - \Phi_m \text{ (n-type; the barrier height of the holes).} \quad \text{(II.4)}$$

2) For minority carriers, the model is the classical description of minority carrier surface recombination. The meaning of the velocity parameter is speed of recombination of the minority carrier then. The minority carrier current jc,min behind contact is therefore given by:

$$j_{c,\text{min}} = \text{qS}_c(c - c_0) \quad \text{(II.5)}$$

Where c denotes concentration of the electron or hole, and the*c0*denotes the concentration of the balance of electrons or holes in contact with the back.

3) The metal work function ϕ_m (for majority carriers) can be entered by the user. However, the user can also choose the flat "strips" option. In this case, SCAPS calculates for each temperature the metal work function ϕ_m in such a path that the flat band conditions predominate:

$$\Phi_m = \chi + \ln\left(\frac{N_C}{N_d - N_a}\right) \text{ (n-type)} \quad \text{(II.6)}$$

$$\Phi_m = \chi + E_g - \ln\left(\frac{N_C}{N_a - N_d}\right) \text{ (p-type)} \quad \text{(II.7)}$$

Here, *Nd* represents the shallow donor concentration and Na for the shallow acceptor concentration, specified in the layer definition. Although this option does not correspond to a physical situation, it allows the user to define a perfect ohmic contact conveniently.

4) All parameters relevant to back contact are assumed to be independent of temperature.

II.2.4. Semiconductor layers

If the (add layer) button is pressed in the solar cell definition panel (Figure II.3), the layer characteristics can be defined in a new screen. The user can now enter the layer name and properties.

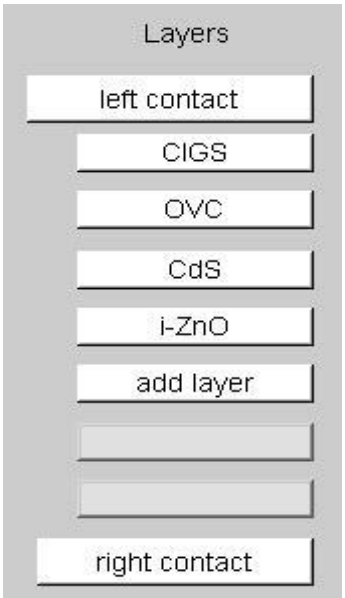

Figure II.3: The Semi-conductor's layers.

When the right mouse button is clicked, with the cursor placed at one of the layers of the semiconductor, a menu appears which allows the user to duplicate and remove an already existing layer. allows the user to duplicate and remove an already existing layer. When the (duplicate) option is chosen, the new layer is inserted below the already existing layer. A new interface is created between the recently created layer and the previous one. When the (remove) option is chosen, the selected layer and the previous interface are removed from the structure.

Remarks:

1) The densities of states in the conduction band and the valence band, NC and NV, depend on temperature as:

$$N_C(T) = N_{C0}\left(\frac{T}{T_0}\right)^{1.5} \quad \text{(II.8)}$$

$$N_V(T) = N_{V0}\left(\frac{T}{T_0}\right)^{1.5} \quad \text{(II.9)}$$

Where the reference temperature T0 equals 300 K. The reference evaluates NC0 and NV0 at room temperature are the values to be specified. The thermal velocity vth(T) depends on temperature as:

$$v_{\text{th}}(T) = v_{\text{th}0}\left(\frac{T}{T_0}\right)^{0.5} \quad \text{(II.10)}$$

Again, the value v_{th0} at ambient temperature is the specified value.

2) The diffusion coefficient is set to kT0 times mobility. The diffusion coefficient and mobility are independent of temperature.

3) The optical absorption constant $\alpha(\lambda)$ of a layer with band gap Eg is given by:

$$\alpha(\lambda) = \left(A + \frac{B}{h\nu}\right)\sqrt{h\nu - E_g} \quad \text{(III.11)}$$

Where $h\nu$ is the energy of the photon, and A and B are constants defined.

If the user presses the button (default 1), he can define the properties of (SRH) recombination in the charge layer of the semiconductor. The defect can be removed by clicking the right mouse button on the defect button to be cleared and choosing the (remove) button.

II.2.5. Defects and recombination

1) The "neutral defect" is an idealization of a defect that contributes to (RSH) recombination but does not contribute to the space charge region. In the case of a (neutral fault), only the product σ and Nt affects the solutions dc and ac (through the lifetimes of the carrier;

n for example is given by $1/(\sigma_n.Nt.vth)$): in this case, the centers of the defect contribute to recombination but not at the space charge zone.

2) The lifetime is displayed only when there is a single level of the defect, uniform in space.

3) All parameters in the default menu are assumed to be temperature independent.

4) The user must specify the recombination somewhere, at least in one place (in a layer or at an interface). If it does not do so, a failure of convergence will result in non-equilibrium conditions (non-zero voltage, and/or illumination).

Table II.1 gives some defects properties. Depending on the nature of the energy distribution, some parameters have different meanings as seen in Table II.2.

Table II.1: Some defects properties [4].

Properties	Description	Value	By default	Unit
Kind	type of defect	-giver -acceptor -natural	Natural	
Sigma n	Cross section electron capture	Digital	1.0E-15	cm2
Sigma_p	Capturing cross section of hole	Digital	1.0E-15	cm^2
Distribution Energy	Fault distribution type	-alone -Uniform -cb vb tail -gauss	Alone	
And	trap energy level respect with the valence band	Digital	0.5	eV
Ekar	Energy characteristic	Digital	0	eV
Profile	Special variation of defect density	-constant -Linear -Exponential	constant	
Lkar	Length characteristic	Digital	0.1	µm
Nleft	max. Defect concentration for layer rightness	Digital	1.0E+14	/cm3 Or /cm3.eV
Nright	max. Defect concentration for the left of the layer	Digital	1.0E+14	/cm3 /cm3.eV

Table II.2: Energy distribution of some defects. [4]

Energy distribution	**Alone**	**Uniform**	**Valencia Band Cue**	**Conduction band tail**	**Gauss**
And	Energy levels	Energy distribution	bottom of the tail	the top of the tail	Energy distribution
Ekar	no meaning	total width of distribution	the characteristic energy (the axis energy)	the characteristic energy (the axis energy)	total width of distribution
Nleft, Nright	density in /cm3	Density distribution constant in /cm3eV	Density distribution constant E=Et in /cm3eV	Constant density distribution in E=Et in /cm3eV	Density distribution constant E=Et on /cm3eV

For each fault distribution an energy axis is calculated with 41 equidistant energies, as:

Table II.3: Equidistant energies.

Distribution Type	The range of energy since	Until	*N(E)* =
Uniform	**And**– Ekar/2	**And**+Ekar/2	*NOT*
vb tail	**And**	**And**+ 7.Ekar	*NOT*.exp(- (E-Et)/Ekar)
cb tail	**And**	**And**- 7.Ekar	*NOT*.exp(- (Et-E)/Ekar)
Gauss	**And**- 3.Ekar	**And**+ 3.Ekar	*NOT*.exp(- ((E-Et) / Ekar)2)

The concentration N in the table above is calculated from Nleft, Nright and Lkar, as:

Table II.4: The concentration N(x).

Spatial profile	*N(x)* =	Noticed
Constant	**Nleft**	**Nright**and Lkar are ignored
Linear	**Nleft**+ *(***Nright**-**Nleft***).(x-x0)/***d**	**Lkar**is ignored
Exponential	*HAS*.exp((x-x0)/Lkar) + B	*HAS*and B are calculated as N(x0) = Nleft and *N(x0+***d***)* =**Nright**

Here the x0 is the spatial coordinate of the left side of the layer, and x0+d that of the right side. If, in the case of an exponential profile, no value for Lkar is specified, an equal defect concentration to 0 will be assumed.

When all the parameters are set, you can add the layer with all its properties to the already existing structure by pressing the "accept" button.

II.2.6. Interface between layers

Between two layered poses we can define the characteristics of the interface by clicking on the right of the rectangle of two layers. Another 3 possible faults can be set by clicking the "defect1,2,3" button.

When the structure is completely defined, the definition file can be saved by clicking the "Save button". When the "OK button" is clicked the energy band panel is shown with different graphics (Figure II.4).

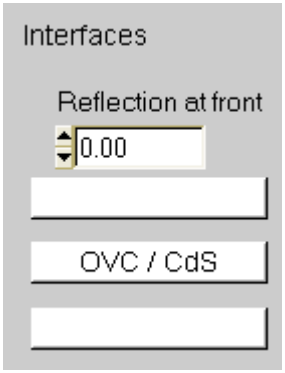

Figure II.4: The interface between the layers.

Table II.5: Some defects properties and the interface between the layers.

Name	Description	Value	Default	Unit
Kind	Fault type	Giver acceptor natural	natural	
Sigma_n	Electron cross-section capture of the conduction band	Digital	1.0E-15	cm2
Sigma_p	Capturing cross section hole of valence band	Digital	1.0E-15	cm2
Energy distribution	Fault description type	Single Uniform tail cb vb gauss	single	
And	trap energy level respect with the valence band	Digital	0.5	eV
Ekar	Energy characteristic	Digital	0	eV
NOT	max. Defect concentration	Digital	0	/cm2 gold/cm2.eV

Remarks :

1) The energy parameters have the same meaning as in the last section.

2) The interface recombination velocities $S_n = N_i\sigma_n v_{th,n}$ et $S_p = N_i\sigma_p v_{th,p}$ are shown only when there is a single energy level interface state. When the thermal velocities of the two layer formations at the interface have different values, there are different values for the interface recombination velocities of carriers coming from the left or the right.

3) If not explicitly stated otherwise, all parameters of the semiconductor layers and interfaces are assumed to be independent on temperature.

4) The model for interface transport is thermionic emission. The thermal velocity of the transport interface equals the smaller thermal velocity of the two neighboring layers.

5) Reflection of photons at interfaces is not taken into consideration.

II.2.7. Front Contact

The front contact is specified in the same way as the rear contact.

II.3. Numerical parameters

Some numerical parameters are also made available in the user interface by the (numeric) button in the solar cell definition panel: the maximum number of iterations, and clamp values for the electrostatic capacitance and for both quasi-Fermi capabilities. These capacities are not allowed to vary in step by more than the corresponding clamp value during numerical integration. Put these parameter influences on the behavior of convergence in extreme cases where convergence is difficult to obtain. The Figure II.5 presents the numerical parameter window.

II.3.1. Loading and changing an Existing Definition File

To load an already existing definition file click on the "File button" in the Calculate New menu. In this screen the user can view and select their definition file. If he presses the "OK button" he gets to the energy band panel with balance graphics immediately. Return to the action panel, click on the "action button.

If we want to create a new definition file based on an old one, we must click the "create new" button in the calculate new menu as for a new definition file. In this screen the "Load button" allows one to load an existing definition file one after another one can change it as a new definition file.

If the user clicks the 'edit' button in 'calculate new' menu, he can make changes in the properties of his structure in the same way as he defined the properties by making the definition file.

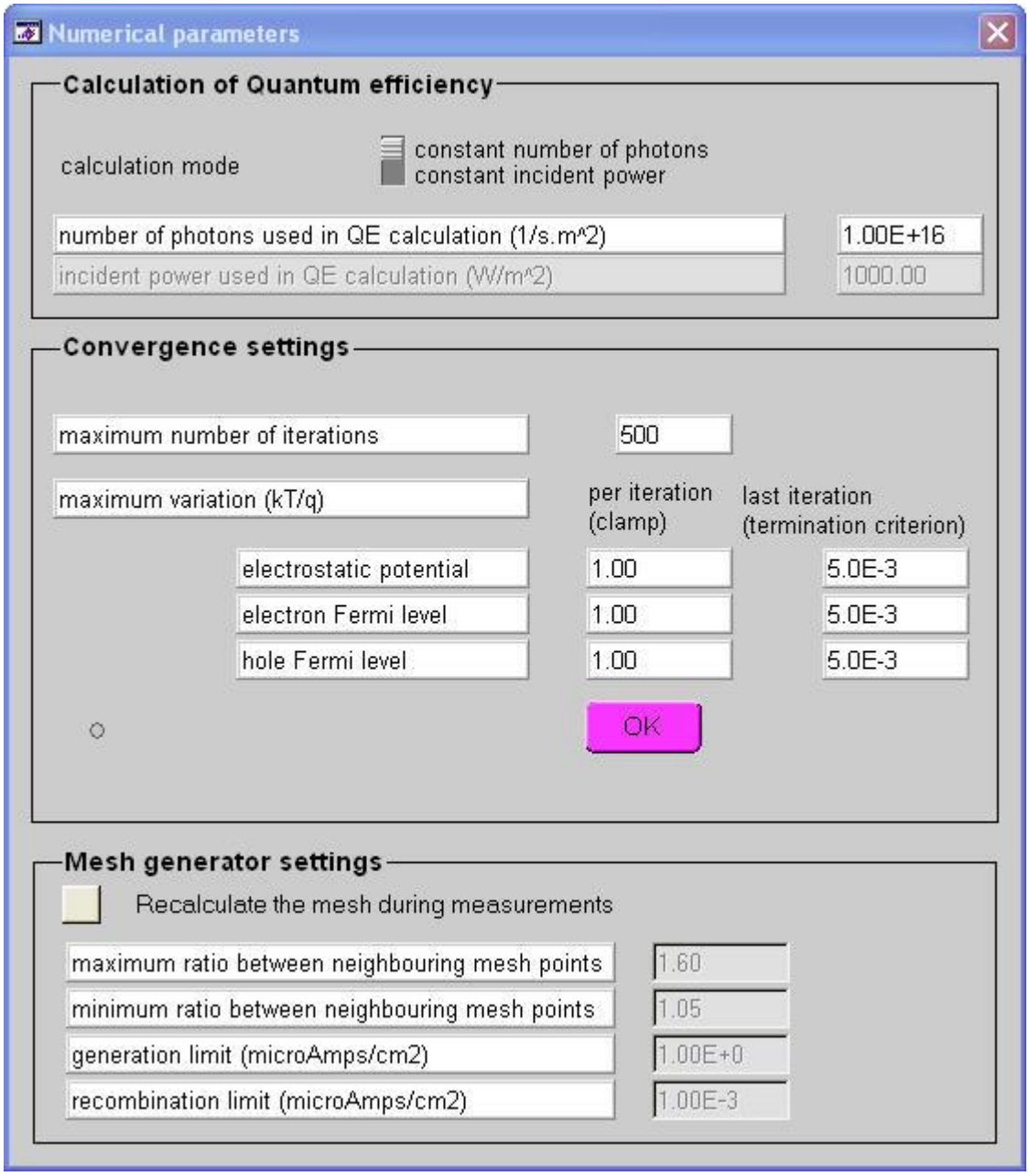

Figure II.5: Numerical parameter window.

II.3.2. Spectrum File

The figure II.6 presents the illumination organization space. We start to select the dark or light mode and in turn from n-side or p-side, contrary we can select spectrum cut off.

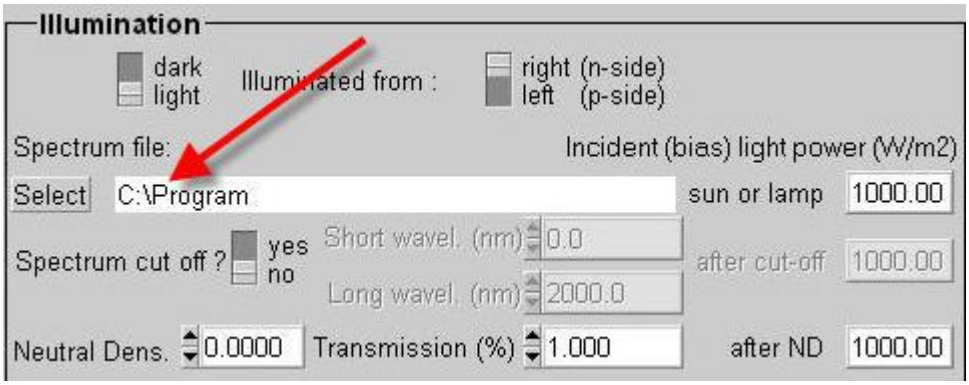

Figure II.6: Illumination organization space.

C:\SCAPS\AM1_5G.spe: AM1.5 global spectrum

C:\SCAPS\AM1_5D.spe: AM1.5 direct spectrum

Other spectrum files can be user defined. The spectrum file is an ASCI - files. The first line contains the number of wavelengths that appear in the spectrum file. This row is followed by two columns immediately. The first column specifies the wavelength λ (nm), the second column contains the power of the incident light W (Watt/m^2) in an interval of the wavelength around λ (the number of photons ' wavelength incidents between λ-$d\lambda/2$ et λ+$d\lambda/2$ is set equal to 5.035×10^{15} W λ $d\lambda$. The maximum number of wavelengths that appear in the spectrum file is 100 mW/cm^2.

II.3.3. Importing digital simulations

The problem is in the problem definition file. The requested calculations are put in the action "list" in the action panel (see below). After creating, editing or loading a problem definition file, you can return to the action panel. When "cancel" is pressed, no calculation is performed, but the edited cell structure stays in active memory. When "OK" is pressed, the calculation of the defined problem is imported immediately, and the energy band "panel" is displayed. You can return to the action panel by pressing the action button.

Figure II.7 presents the .def file export tool when we can export the previous defined programs or some example programs.

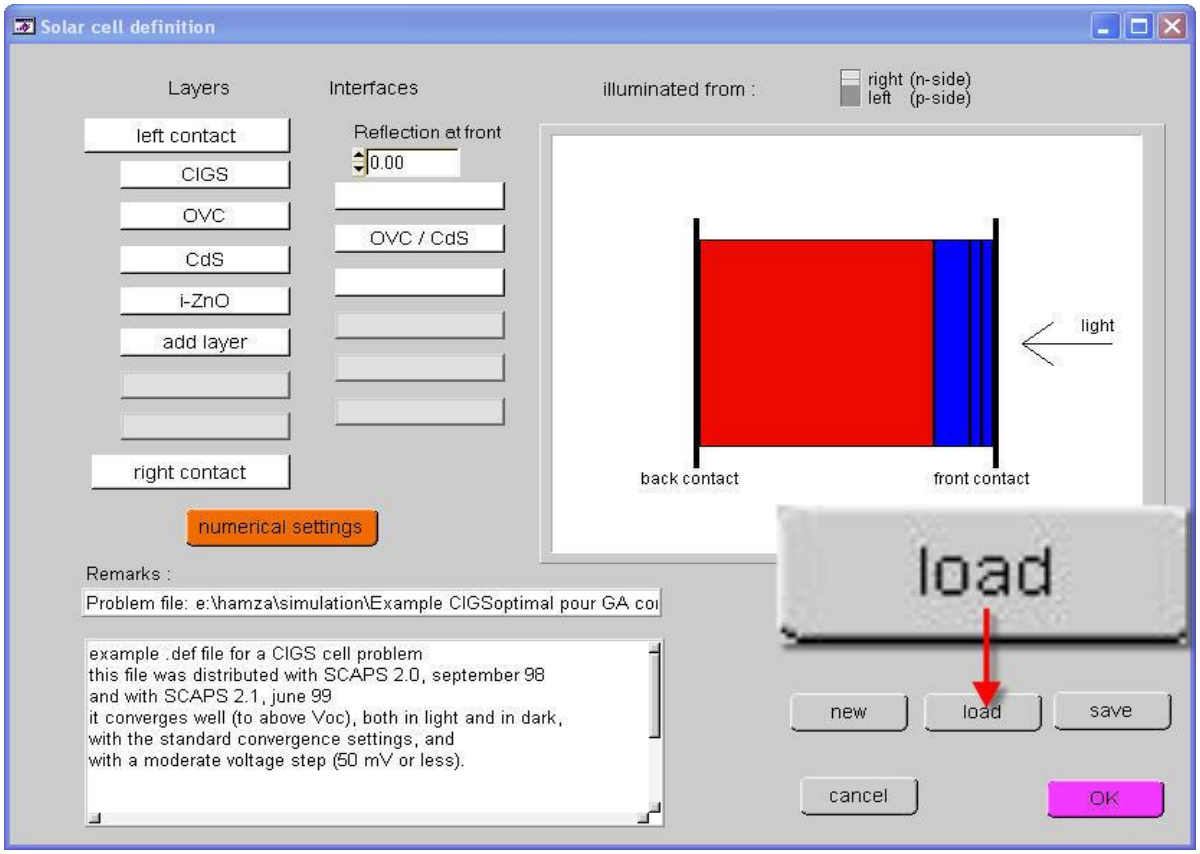

Figure II.7: The .def file export tool.

The action panel allows as to specify an operating point defined by temperature (K), DC voltage (V), illumination conditions (dark spectrum, full spectrum, natural density and/or bandpass filter) and an ac frequency, as seen in Figure II.8.

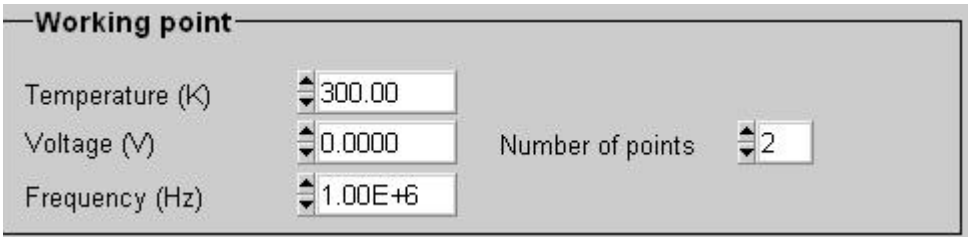

Figure II.8: Operating point determination space.

The spectrum stop option simulates the use of a long bandpass filter and a long stop filter in the DC-illumination condition. This option is effective only when Spectrum Off is set to yes, and when Illumination is on (i.e. "dark" = none). Spectrum stopping affects all calculated curves (although many cell types are not very sensitive to it).

However, the spectral response does not fall to zero in regions where the spectrum is dead. The spectral stop affects the condition of the applied illumination (influence dc, the light source), while the spectral response is calculated as the response to a small source of light from the ac,

superimposed on the light from the bias (simulate the measurement installed with chopped light of a monochromatic and applied light).

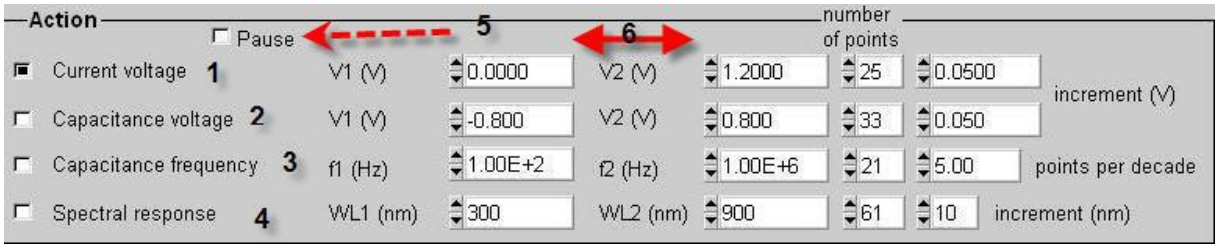

Figure II.9: Parameter adjustment space.

Using the parameters adjustment space, presented in Figure II.9, the following characteristics can be calculated:

1) Current versus Voltage (I-V characteristic): from a specified voltage V1 to V2 (V) in steps n, for the illumination conditions and temperature specified in the operating point (wp).

2) Capacitance against voltage (C-V curves): from a specified voltage V1 to V2 (V) in step n, for the conditions of illumination, temperature and ac frequency, specified in the operating point (wp).

3) Capacitance versus frequency (C-V curves): from a specified frequency f1 to f2 (kHz) in steps n (equidistant on a logarithmic scale) for illumination conditions, the dc influence voltage and temperature specified in the active point.

4) Quantum efficiency QE versus wavelength: from a specified wavelength 1 to 2 (nm) in steps n for the (biased) illumination conditions, the DCs influence voltage and operating point temperature.

Each new calculation begins with the calculation of the equilibrium band diagram (V=0, dark); If the operating point specifies illumination, next the band diagram of the short circuit is calculated. Each next calculation starts from the previously calculated solution. The order of calculation is: first the operating point, then IV, CV, Cf and QE curves, if requested. When the pause button shown in the figure above with arrow numbered 5) in the action panel is enabled, the program stops after each calculation, and resumes when the (continue) button is pressed in the action panel action or in the energy bands panel. When (pause) is turned off, all required calculations are executed one after the other.

Convergence problems can occur when the operating point voltage is too different from zero (= the previously balanced voltage and perhaps Jsc calculation) (see Figure II.10). To overcome this problem, SCAPS allows specifying several steps to be taken to evolve from zero voltage to the operating point voltage. Problems can also occur if the initial calculated IV or CV voltage is too different from the operating point voltage. In this case we can put the influences of the dc voltage equal to the operating point at the starting point of the calculated IV or CV, so that the calculations of IV or CV can start with the correct solution.

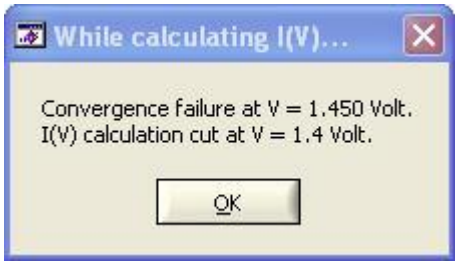

Figure II.10: Convergence failure window.

Once a calculation is finished, it is possible to consider the corresponding IV, CVS, Cf and QE panels. The most recently calculated energy band diagram panel shows. If a Cf calculation is made, SCAPS automatically shows the AC panel.

By pressing the calculate button in the action panel, a new calculation with the same definition file, but with a different action list can be done. If the operating point is the same as for the previous calculation, short circuit and influence of balance conditions will not be recalculated.

II.4. The Action Panel

The Figure II.11 presents the action panel. In this panel the following pieces of information are available:

- The definition of the active point (see above);
- The definition of the action list (see above);
- Set calculation mode: "take a break" between calculations or not (see above);
- Put the problem definition: the "calculate new" button (see above);
- Carry calculations from a new action list: the "calculate next" button (see above);
- "continue" to calculate next action list operation, when "pause" is allowed
- "stop" to stop a calculation that is carried from outside;

- "clear previous" clear previously calculated graphs;
- "graphs" activate the energy bands panel from which in turn we can navigate to all the other graphic panels (IV, CV, Cf and QE).

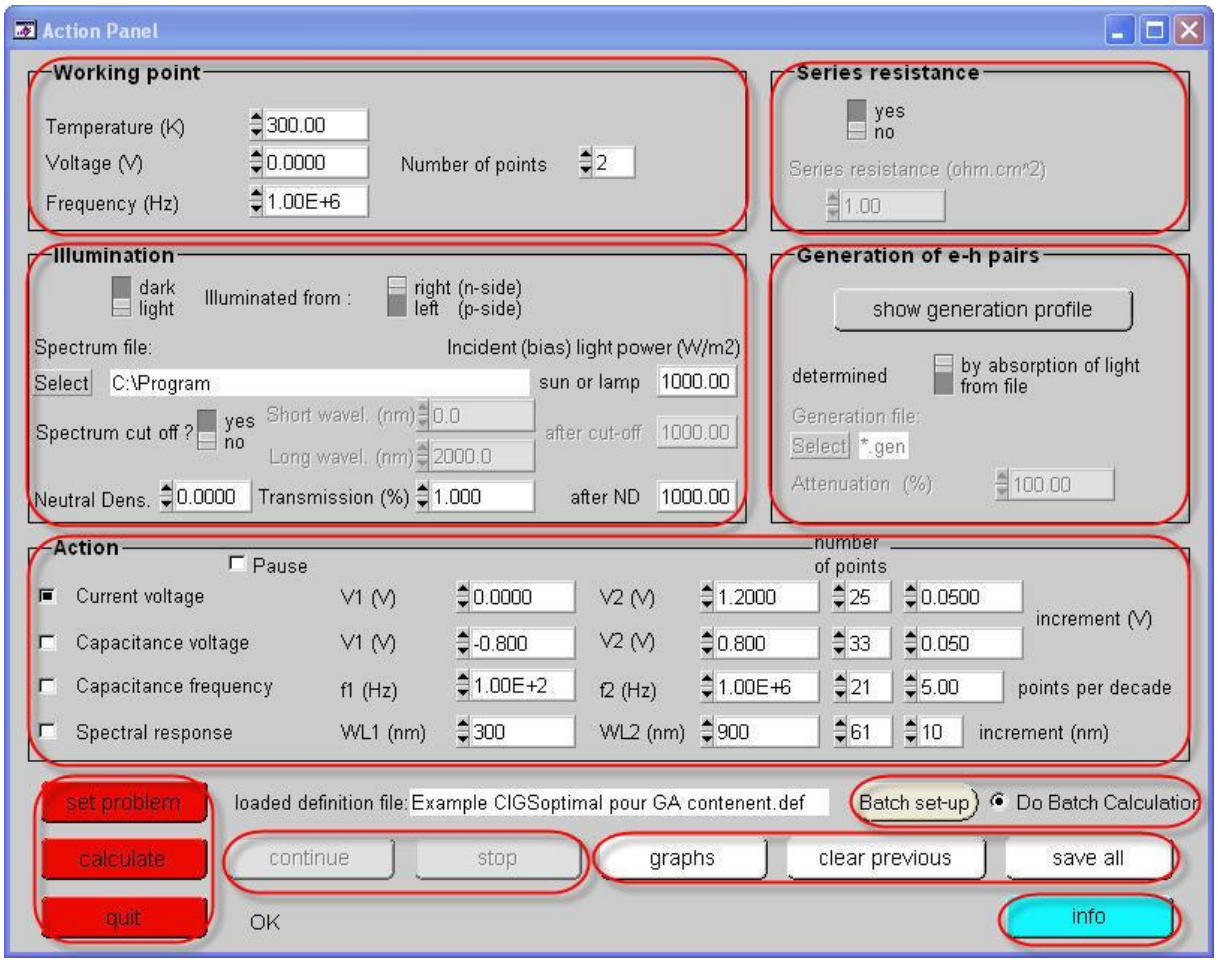

Figure II.11: The Action panel.

- "save all" to always save the results of all preformed calculations in a text file; The data in the text file is separated by labels, and can be cut and can be pasted into an extent sheet or graphics program;
- "exit" exit from SCAPS-1D. This is the only correct way to leave SCAPS!

II.5. Energy band panel

The Figure II.12 presents the energy band panel. In this panel the following buttons are available:

- "continue": resume a calculation stopped by the pause option;

- "save": save the energy band calculation results to a text file;
- "plotter": plot the content of the panel to the Windows default printer. Note: this is a low "quality footprint" screen, only for consideration and purposes of discussion. For presentation purposes, it is best to save the calculation in a text file, and use this file to make presentation graphics with the preferred graphics program;
- "action": return to the action panel.

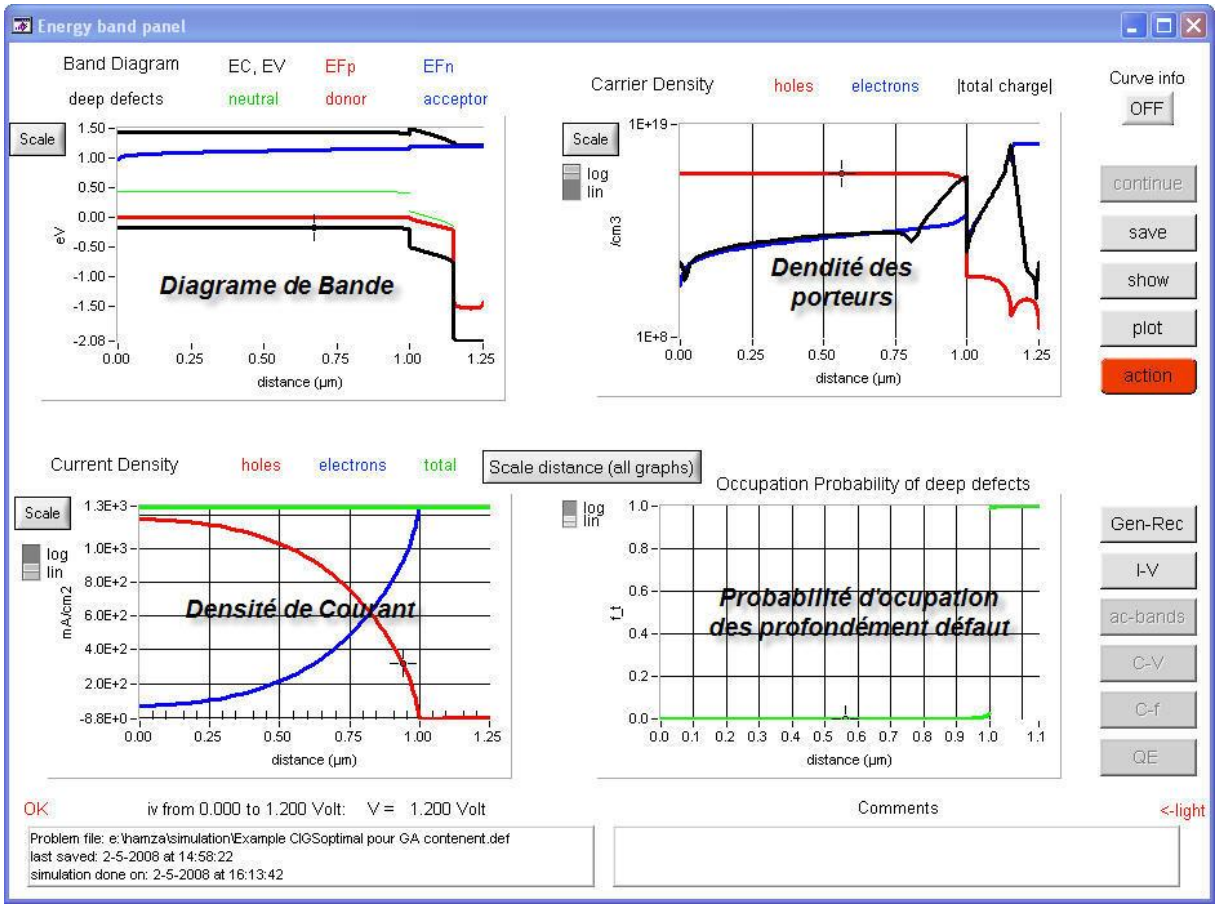

Figure II.12: The energy band panel.

The buttons " **IV→**", **QE→** ", **AC→**", **CV→** " et " **Cf→**", navigate to the indicated graphic panels.

The results of the last calculation of the energy band are shown in four graphs: it is therefore in the illumination and the voltage conditions of the last calculation executed (therefore the active point or the last point of IV, QE,… curves).

There is a cursor utility available in the EB - Panel, and in the other graphics panels too. If you click with the mouse on a point of the graph of your choice you can see the x and y evaluation

of that point in the two small windows in the middle of the screen. The units are the same as the user's units of the axes of the relevant graph.

The first graph (upper left) is the show of the (DC) band diagram: black for conduction and valence line, blue for fermi level of electron, red for fermi level of hole or only red if the fermi levels coincide. The fault levels, if present, also have their color: green for a neutral fault, blue for an acceptor type fault and red for a donor type fault. (in fact, the characteristic energy Ekar of defects is shown). It is easy to discern between defect levels and fermi levels, since defect levels exactly follow the sharp band, while fermi levels do not.

The second graph (upper right) shows the carrier densities as a function of distance: blue for electrons, red for holes, and black for total charge.

The third graph (lower left) is the showing of the current density as a function of distance: blue for electrons, red for holes, and green for total current.

The fourth graph (lower right) shows the probability of occupancy of defects as a function of distance: green for neutral defects, blue for acceptor type, red for donor type defects.

II.6. Panel of IV characteristics

The “continue”, “show”, “plot” and “action” buttons, and the navigation button navigation **“EB→”**, **“QE→”, “AC→”, “CV→”** et **“Cf→”** have the same meaning as in the energy bands panel (see Figure II.13).

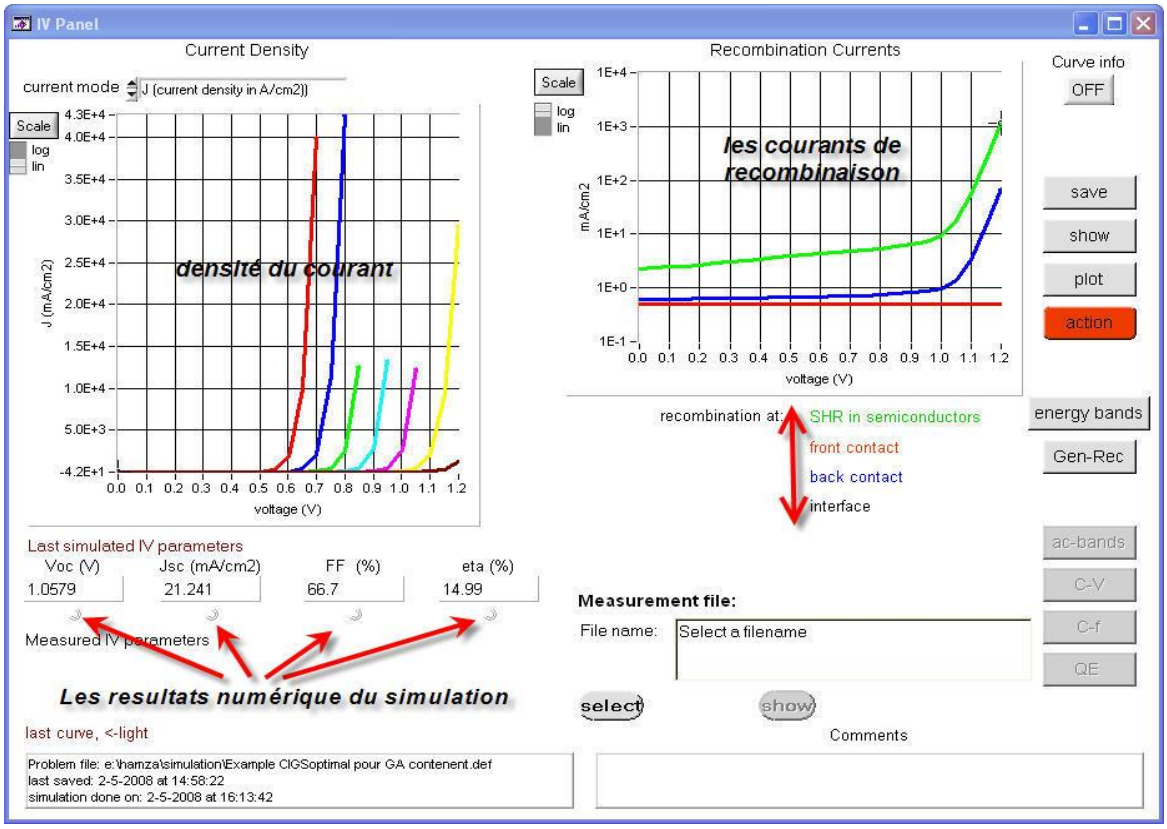

Figure II.13: Panel of JV characteristics.

The "continue", "show", "plot" and "action" buttons, and the navigation buttons and **"EB→"**, **"QE→"**, **"AC→"**, **"CV→"** et **"Cf→"** buttons have the same meaning as in the energy bands panel.

The first graph (left) is the exposition of the current density as a function of the applied voltage. The first calculation (that is, after "calculate again", the problem has settled and "OK"), the IV curve (when calculated) is plotted in red. Each next calculation (so after a "calculate next" or after another "calculate again"), a new IV - curve is added (when calculated), in a different color. The color order is: red, blue, green, cyan, magenta, yellow … (14 colors). When "Previous Clear" is pressed on the Action panel, all IV curves are cleared, and the color starts again from red. The second graph (right) is the exposure of the recombination current as a function of the applied voltage:

The new utilities on SCAPS are:

❖ **Batch calculation**

If you want to know the influence of one or more parameters on the solar cell characteristics, using this new option does it easily, it just involves clicking on the Batch button and setting the

parameters you want to vary. Variations can be simultaneously made. The Figure II.14 presents the Batch tool to do the Batch calculation and the panel to input different material parameters.

We must select the instruction (Do Batch Calculation) to perform the batch calculations.

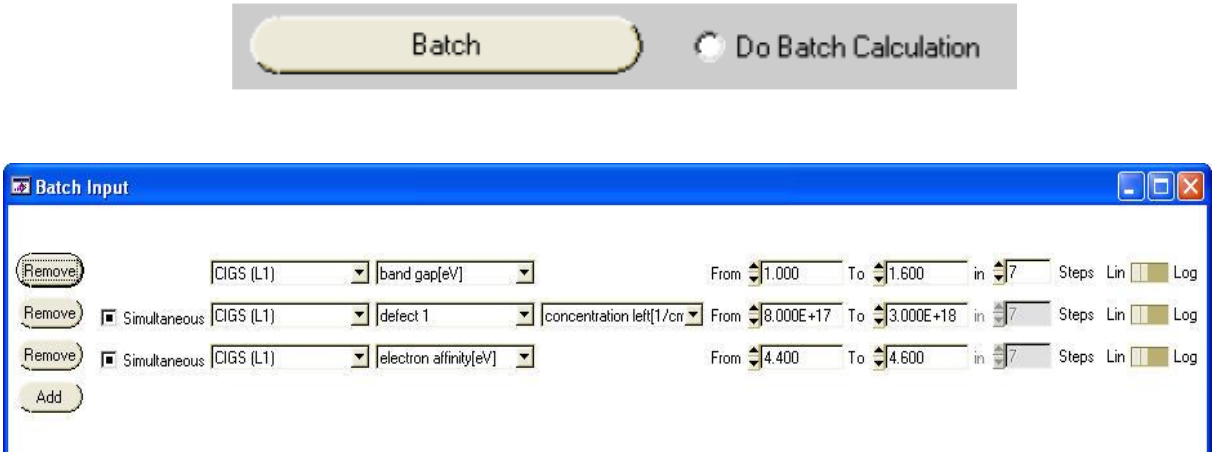

Figure II.14: The Batch tool.

❖ The Tunnel effect tool

Currently two tunneling mechanisms are built on SCAPS 2.6 intra band tunneling and tunneling to interface states to put the tunneling option you must click the corresponding button on (the interface states-panel) (see Figure II.15).

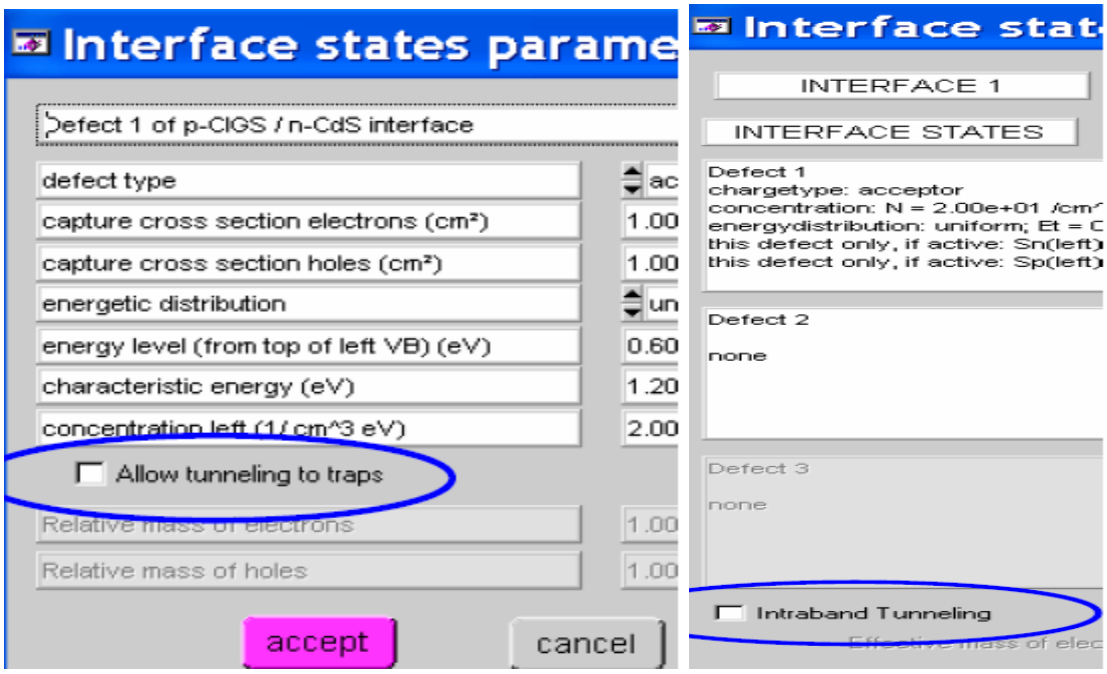

Figure II.15: The tunnel effect tool.

II.7. Conclusion

SCAPS-1D tool, one of the most popular simulators in the world of photovoltaic field simulations, because it is simple and easy for an electronics engineer, who wants to model cells in thin layers of this kind. The results and configurations are valid on a file with a specific extension but accessible in text format and this makes all the operations of (copying, pasting) the results easier, again with the type of data selection being vertical or horizontal.

The possibility of opening several SCAPS-1D windows simultaneously which gives us the power to perform more than one task, depending on the power of the PC and the stability of SCAPS-1D. The latter represents disadvantages for its functionality due to the risk of loss of results. The processing speed is very fast, especially with the new batch tools which allow the user to vary one or more parameters at the same time or separately.

The SCAPS-1D interface is simple but the graphical representation is simpler because the (Zooming) operations are done by hand and also the exploitation of its graphs.

References

[1] A. Niemegeers, S. Gillis et M. Burgelman, 1998. " UN programme de l'utilisateur pour simulation réaliste d'heterojunction du polycrystalline cellules solaires: SCAPS-1D ", Débats de la 2e Conférence Mondiale sur Conversion D'énergie Photovoltaïque (Wien, Österreich, july 1998), pp. 672-675, JRC, Ordre européen,

[2] M. Burgelman, P. Nollet et S. Degrave, semi-conducteur du polycrystalline du 1999. " Modelage cellules " solaires, (a invité) a présenté à la Société de la Recherche des Matières européenne, E-MRS, Strasbourg, France.

[3] A. Niemegeers et M. Burgelman, modelage 1996. " Numérique d'ac caractéristiques de CdTe et CIS cellules " solaires, Proc. 25e IEEE Conférence des Spécialistes Photovoltaïque (D.C. de Washington, april 1996), pp. 901-904, IEEE, Nouveau York,

[4] M. Burgelman, K. Decock, S. Khelifi and A. Abass, (2013) . "Advanced electrical simulation of thin film solar cells", Thin Solid Films, **535** 296-30

[5] K.Decock, P. Zabierowski, M. Burgelman, (2012) "Modeling metastabilities in chalcopyrite-based thin film solar cells", Journal of Applied Physics, 111 043703

Chapter III

Results and Discussions

III.1 Introduction

Semiconducting metal oxides have been a focus of fundamental research recently [1–4]. CuO and Cu_2O absorbers have emerged as promising materials for optoelectronics and these materials are the possible solution for cheap and competitive solar cells construction.

In the literature there are few reports on solar cells based on copper oxide as active layers. The conversion efficiency is the most important property in the PV domain [5,6]. Although the theoretical limit of the energy conversion efficiency of Cu_2O solar cell is ~ 20% [7], the highest efficiency obtained on substrates Cu_2O solar cell is 3.83% [8].

In this work, we present a numerical study of the CuO and Cu_2O thin film solar cells using Solar Cell SCAPS-1D Program. It is used to calculate the photovoltaic parameters, the most important: Open-circuit voltage (V_{OC}), Short-circuit current density (J_{sc}), Fill Factor (FF) and efficiency (η) under standard illumination (AM1.5G, 100 mW/cm^2, 300K).

The purpose is to study the effect of different physical paramaters such as: Thickness, the acceptor concentration and Defect concentration on the performance of the solar cells. Towards this goal: the current density (J_{sc}) and efficiency (η) have been calculated. Additionally, we examined the quantum efficiency QE.

III.2. Modeling of substrate CuO and Cu_2O solar cells

The conventional structure of CuO and Cu_2O solar cells consists of a glass substrate, a molybdenum back contact layer, a CuO or Cu_2O absorber layers, a CdS buffer layer and finally a transparent conducting oxide front contact ZnO layer. This structure is designed to optimize light absorption, charge transport, and collection in CuO and Cu_2O absorber layers.

In the conventional structure, the n-type CdS buffer layer is inserted between the ZnO window layer and p-type CuO and Cu_2O absorber layers to make a high-quality p-n junction in the interface [9]. The n-type CdS buffer layer was taken using 0.1 nm-thick and 2×10^{17} cm^{-3} donor density with a gap of 4.2 eV. The CuO and Cu_2O absorber layers are a p-type semiconductor with 3 μm-thick and 2×10^{16} cm^{-3} acceptor density [10] with a moderate gap E_g = 1.51 eV and E_g = 2.15 eV [11]. The degenerate ZnO(n+) window layer was taken as a wide band-gap Transparent Conducting Oxide (TCO) semiconductor (3.30 eV), with 0.1 nm-thick and 1×10^{19} cm^{-3} donor density [12]. In the proposed structures, a schematic view of the conventional CuO and Cu_2O solar cell structures were displayed in Figure III.1.

In the first part of this work, we will study the effect of CuO and Cu_2O layer thicknesses and doping concentration on the current density-voltage (J-V) characteristics and quantum efficiency (QE) of the conventional cell ZnO/CdS/CuO and ZnO/CdS/Cu_2O structures.

III.3. Physical model and simulation parameters

As we mentioned above, the SCAPS-1D simulator allows the solution of a set of basic semiconductor equations consisting of the Poisson equation and the continuity and transport equations for electrons and holes [13], the Newton method was selected for solving the basic semiconductor equations in the software as a default method. The band-gap E_g of CuO and Cu_2O alloys was calculated using the data mentioned in Table III.1 [14].

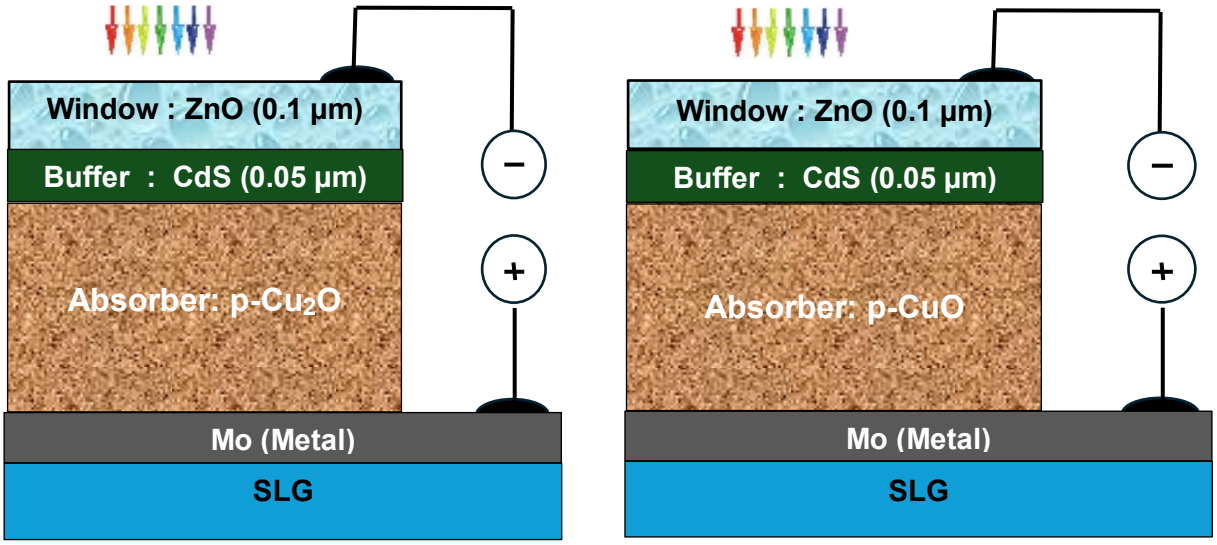

Figure III.1: Cu_2O and CuO solar cell structures.

The input parameters of each layer of the proposed structure are summarized in Table III.1. These parameters are the thickness *w*, the permittivity constant εr, the band-gap E_g, the electron affinity χe, the electron/hole mobility μ_n/μ_p, the effective density of states in conduction/valence band N_C/N_V, and the donor/acceptor concentration N_D/N_A. At the front contact, the reflection was neglected. The values of the surface recombination velocity for holes/electrons S_n/S_p at front and back contacts were 1×10^7 cm/s.

Because all the layers are polycrystalline, they contain a wide range of defects [15]. Therefore, For CuO and Cu_2O materials, we used tow Gaussian deep donor defect distribution, and tow Gaussian deep acceptor defect distribution for ZnO and CdS layers. The donor and acceptor defect distributions are provided by SCAPS-1D.

$$g_{GA}(E) = N_{GA} \exp\left[-\left[\frac{E_{GA}-E}{W_{GA}}\right]^2\right] \quad \text{(III.1)}$$

$$g_{GD}(E) = N_{GD} \exp\left[-\left[\frac{E-E_{GD}}{W_{GD}}\right]^2\right] \quad \text{(III.2)}$$

Where E is the defect energy, the subscripts (G, A, D) stand for Gaussian acceptor and donor defect states, respectively. The effective density of states (N_{GA} and N_{GD}), standard energy deviation (W_{GA} and W_{GD}), and peak energy position all characterize the density of states (E_{GA} and E_{GD}).

Copper forms two well-known stable oxides: cupric oxide (CuO) and cuprous oxide (Cu_2O). These two materials have different physical properties, different colors, crystal structures and electrical properties [16,17]. Both forms are a natural p-type semiconductors [18]. The first attempt to use Cu_2O for PV application was done by National Science Foundation and Joint Centre in 1978 [19, 20]. Cuprous oxide Cu_2O has low electron affinity (3.2 eV) [21,22,23], and very high hole mobility [24,25]. Thus, it is suggested as a potential hole transport material in heterojunction based solar cells [25,27]. A few attempts were made to fabricate n-type Cu_2O solar cells, but the achieved efficiency is very low so far [28].

Properties of the materials, used in the simulations are available in the literature. The parameters of Cu_2O, CuO and CdS used in our simulations are listed in Table III.1.

Table III.1: Parameters values of CuO and Cu_2O solar cell structures used in SCAPS-1D [26,29-42].

Material properties	CuO	Cu_2O	CdS	ZnO
Thickness	/	/	0.1	0.08
Band gap [eV]	1.51	2.17	2.4	3.3
Electron affinity [eV]	4.07	3.20	4.2	4.6
Dielectric permittivity (relative)	18.10	7.11	10	9
CB (conduction band) effective density of states [cm^{-3}]	2.2×10^{19}	2×10^{17}	2×10^{18}	2.2×10^{18}
VB (valence band) effective density of states [$1/cm^3$]	5.5×10^{20}	1.1×10^{19}	1.5×10^{19}	1.8×10^{19}
Electron mobility μn[cm^2 /Vs]	100	200	100	100
Hole mobility μp [cm^2 /Vs]	0.1	80	25	25
Shallow uniform donor density N_D [$1/cm^3$]	0	0	1×10^{17}	1×10^{19}
Shallow uniform acceptor density N_A [$1/cm^3$]	1×10^{16}	1×10^{18}	0	0

III.4. Band diagram

The band gap and optical properties of Cu_2O and CuO have already been widely studied in theoretical calculations and experiments [4,43-47]. Experimentally, it is well established that Cu_2O has a direct forbidden gap of about 2.17 eV and a direct optically allowed band gap of 2.62 eV (low temperature values). The CuO material has a direct forbidden gap of about 1.51 eV. The absorption coefficient α for both Cu_2O and CuO absorber films are given by ref [26]. as presented in Figure III.2.

Figure III.3 exhibits the energy band diagrams for both (a) CuO and (b) Cu_2O solar cell structures obtained by simulation.

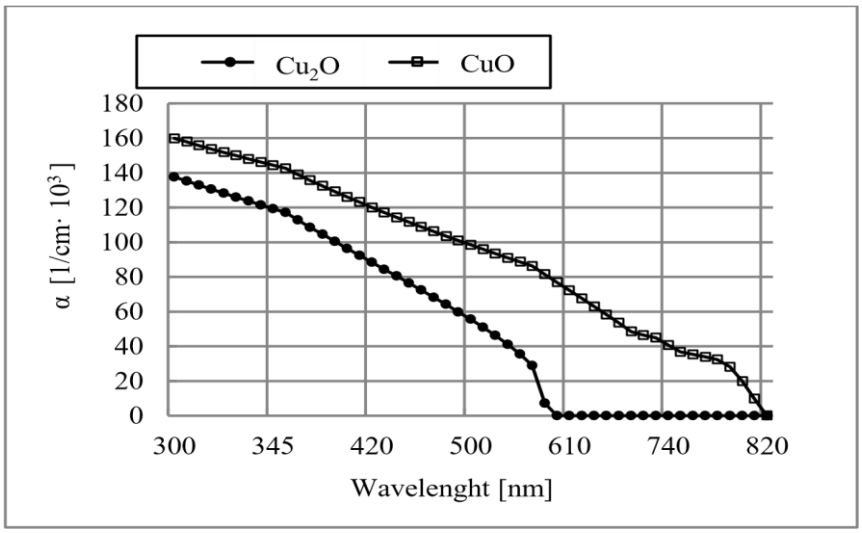

Figure III.2: Absorption coefficient α for both Cu2O and CuO absorber films used in the simulation.

(a)

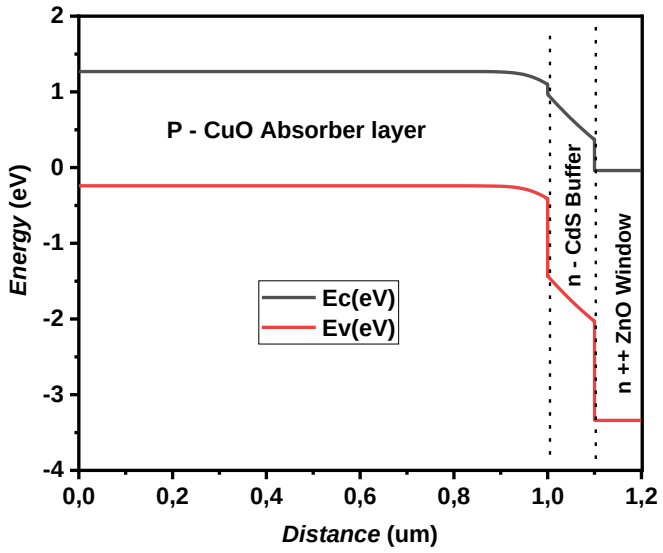

(b)

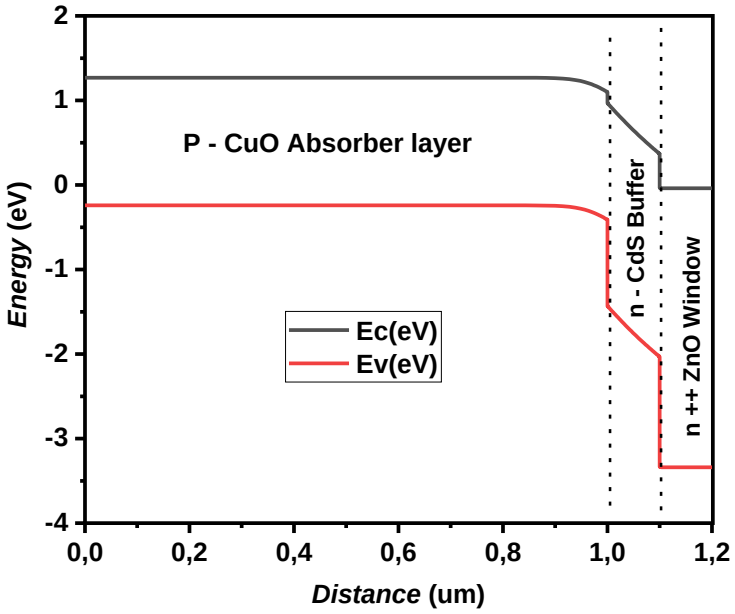

Figure III.3: Band diagram for (a) CuO and (b) Cu_2O solar cells structures used in the simulation.

III.5. Thickness optimization of CuO and Cu_2O absorber layer

In this part, we'll look at the performance of the CdS/Zno/CuO and CdS/Zno/Cu_2O solar cell using the material parameters listed in Table III.1. Figure III.4 shows the evolution patterns of V_{oc}, J_{sc}, *FF* and η of CuO and Cu_2O solar cells as a function of CuO and Cu_2O absorber layer thickness.

When the CuO absorber thickness, *t*(CuO), is increased from 0.1 to 10 µm, J_{sc} rise significantly from 13.2 mA/cm^2 to approximately 26 mA/cm^2 and η increases rapidly from 8.4% to about 21% respectively. V_{oc} reches 1.67V and *FF* reaches 33%.

When the Cu_2O absorber thickness, *t*(Cu_2O), is increased from 0.1 to 10 µm, J_{sc} rise significantly from 6.8 mA/cm^2 to approximately 13.8 mA/cm^2 and η increases rapidly from 2% to about 10% respectively. V_{oc} reches 1.24 V and *FF* reaches 50%.

All photovoltaic properties are nearly identical for a thick CuO and Cu_2O absorber layer (more than 3 µm). This overall behavior is resulted from the increase of the photons absorption and even the increase of the electron-hole generation in the CuO and Cu_2O absorber layers. Therefore, the thickness of 3 µm is chosen as an optimum thickness for CuO and Cu_2O absorber layer for an efficient ZnO/CdS/CuO and ZnO/CdS/Cu_2O solar cells [9]. If the absorber layer

thickness is reduced the back contact will be very close to the depletion region [18]. Additionally, for comparison, similar behaviors of the performance parameters were achieved by Benmir et *al.* [19] and Heriche et *al.* [20].

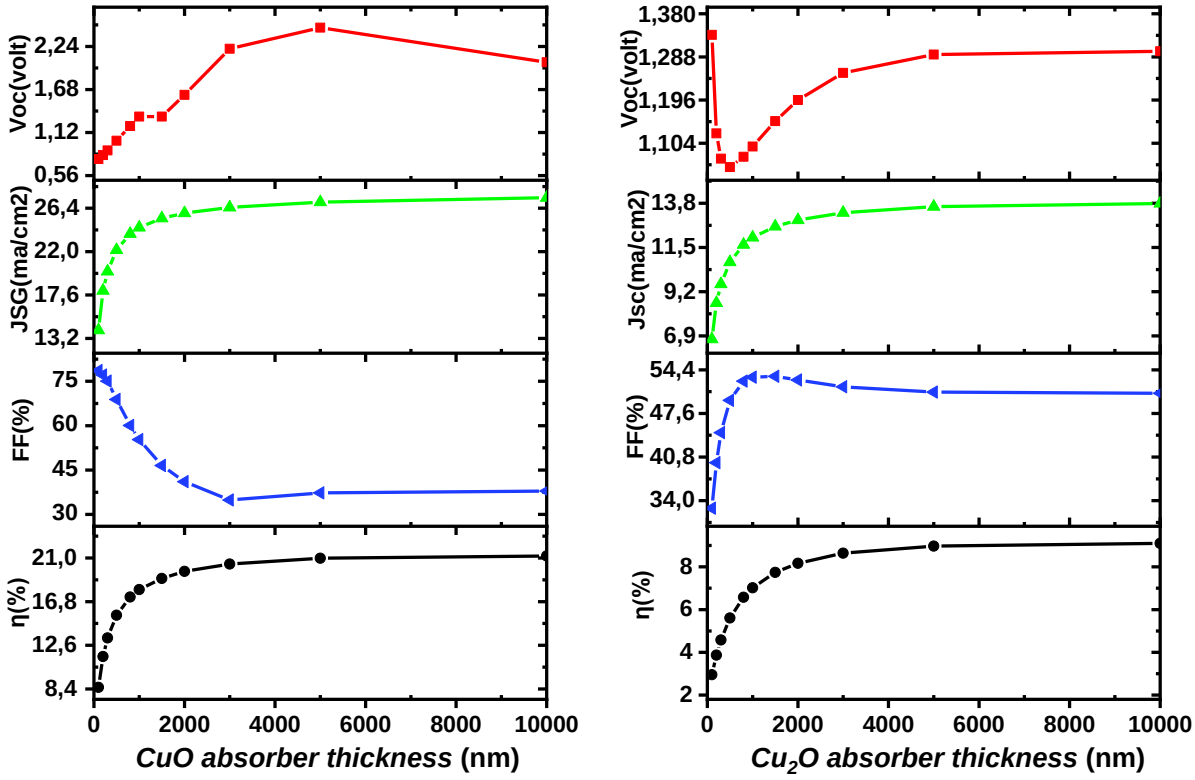

Figure III.4: Cell performance as a function of CuO and Cu_2O absorber layer thickness.

For a better understanding of current losses with increasing the absorber thickness, the quantum efficiency QE was calculated and the results are given in Figure III.5 for CuO and Cu_2O thicknesses varied between 0.1 to 3 µm. For wavelength below 400 nm and above 650 nm all structures show nearly the same behavior. In the region between 430 nm and 850 nm a significant loss is observable. When the thickness increases from 0.1 eV to 3 µm the maximum of quantum efficiency increases. The maximum corresponding to the thickness of 3 µm.

(a)

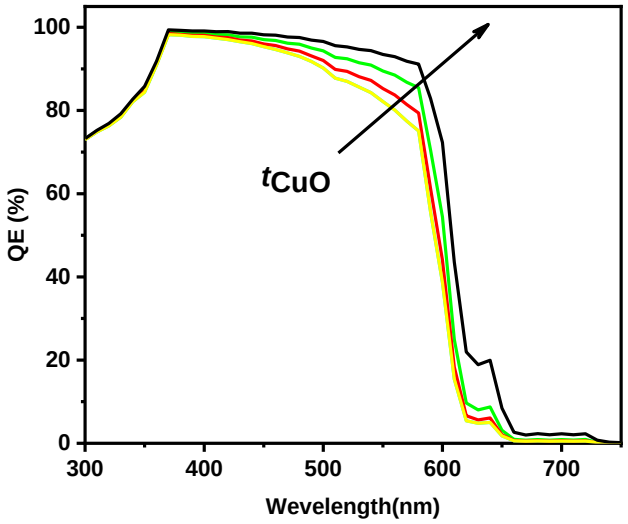

(b)

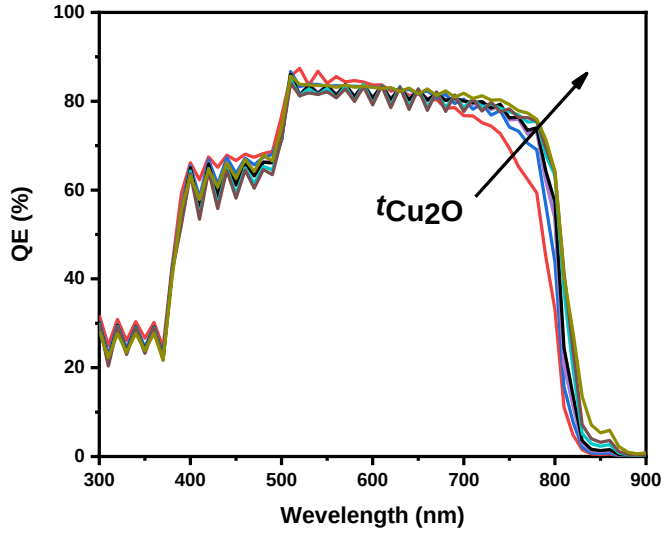

Figure III.5. Quantum efficiency versus wavelength of (a) CuO and (b) Cu_2O solar cell structures.

III.6. Optimization of acceptor density N_A(CuO) and N_A(Cu_2O)

The acceptor concentration of CuO and Cu_2O absorber layers has been discovered to be significant factors that have a direct impact on the performance of CuO and Cu_2O based solar cells. As a result, the absorber layer's acceptor concentration, N_A(CuO), is adjusted from 10^{11} cm^{-3} to 10^{19} cm^{-3}, and the simulated photovoltaic characteristics are displayed in Figure III.6. The J_{sc}

exhibits a very modest drop from 7 mA/cm^2 for a concentration of 10^{11} cm^{-3} to an acceptable limit of 22 mA/cm^2 for a concentration of 1×10^{19} cm^{-3}.

$N_A(Cu_2O)$ is adjusted from 10^{11} cm^{-3} to 10^{19} cm^{-3}, and the simulated photovoltaic characteristics are displayed in Figure III.7. The J_{sc} exhibits a very modest drop from 14 mA/cm^2 for a concentration of 10^{11} cm^{-3} to an acceptable limit of 12 mA/cm^2 for a concentration of 1×10^{19} cm^{-3} , which is caused by an increase in free carrier charge recombination that occurs inside the bulk [21].

On the other hand, V_{oc}, *FF* and efficiency are increased significantly with the increase of $N_A(CuO)$ from 10^{11} cm^{-3} to 10^{19} cm^{-3} whereas the optimum efficiency achieved is 19.5% and in $N_A(Cu_2O)$ is 11% in the acceptor concentration of about 10^{17} cm^{-3}, the $V_{oc} \approx 4.4$ V and $FF \approx 68\%$ and in Cu_2O $V_{oc} \approx 3.3$ V and $FF \approx 22\%$. After this value the structure presents a strong decrease in the V_{oc}, *FF* and efficiency. The result indicates that the $N_A(CuO)$ and $N_A(Cu_2O)$ must be higher than 10^{16} cm^{-3} and lower than 1×10^{17} cm^{-3} to obtain a good performance.

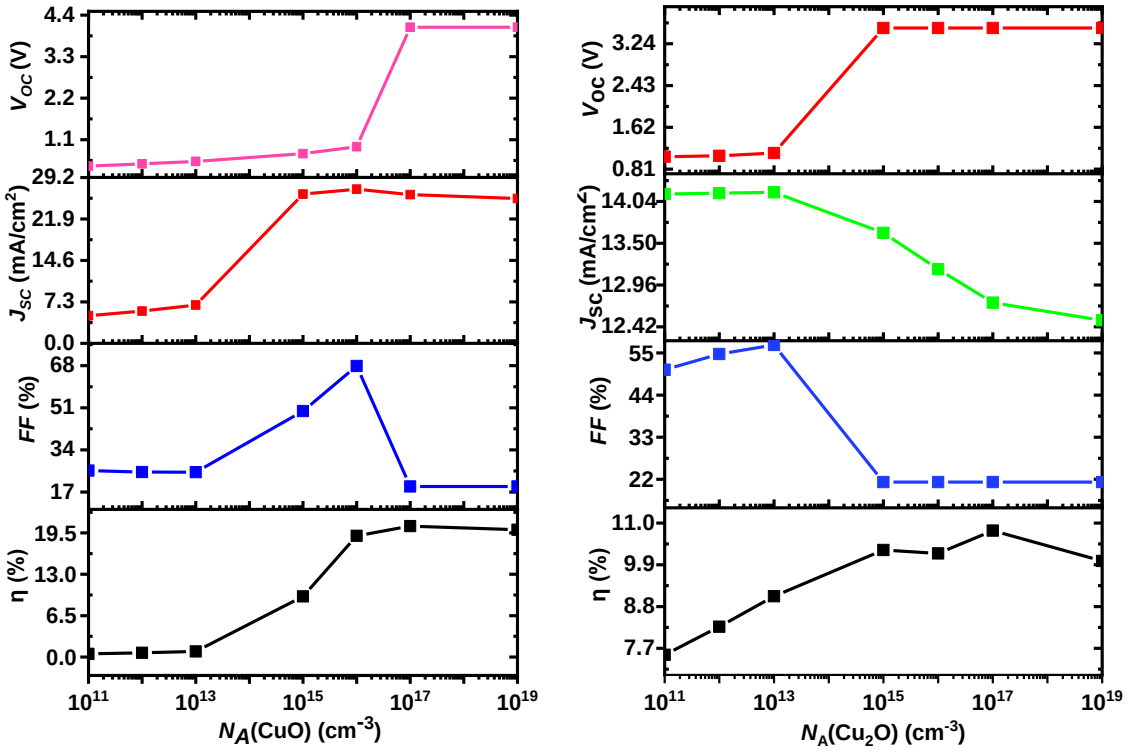

Figure III.6: Effect of acceptor concentration of absorber layer $N_A(CuO)$ and $N_A(Cu_2O)$ on cell performances.

The spectral responses of various acceptor concentrations for Cu_2O and CuO absorber layers were studied and presented in Figure III.7 and Figure III.8, respectively. With increasing $N_A(Cu_2O)$ and $N_A(CuO)$, the spectral response increases in long wavelength region. The quantum efficiency has a maximum value close to 98% under 100 mW/cm^2 illumination between wavelengths varied from 500 nm to 600 nm.

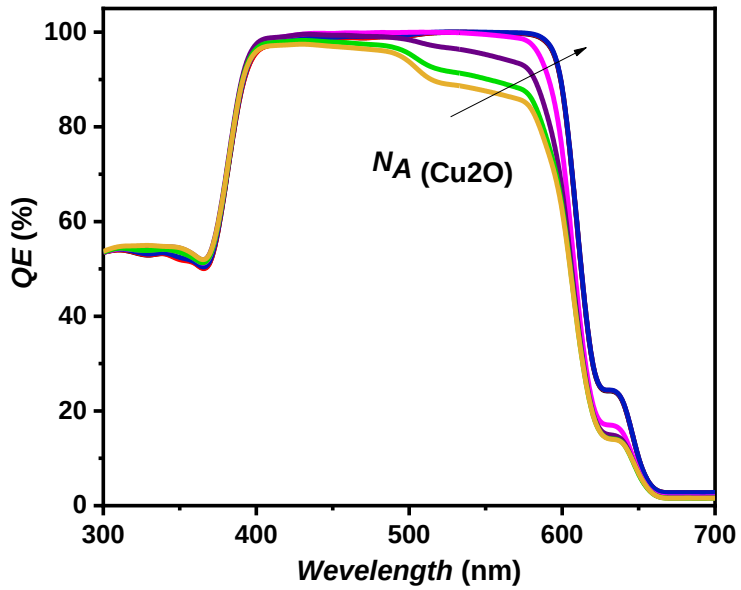

Figure III.7: Quantum efficiency QE of Cu_2O solar cell for various acceptor concentrations, $N_A(Cu_2O)$.

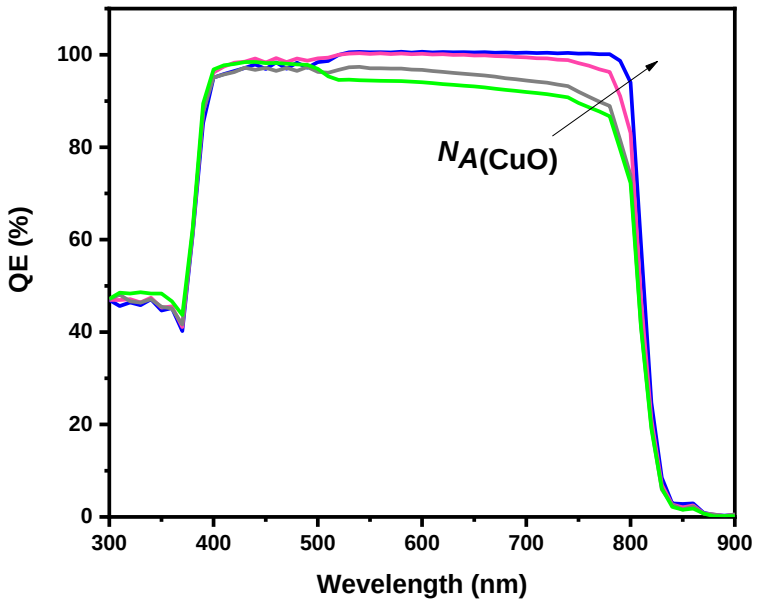

Figure III.8: Quantum efficiency QE of CuO solar cell for various acceptor concentrations, $N_A(CuO)$.

III.7. Influence of defect state density of CuO and Cu_2O absorber layers

The conversion efficiency of CuO and Cu_2O solar cells is drastically influenced by defects concentration (trap defects density N_T) in the bulk of absorber layers. The simulation results of CuO and Cu_2O solar cell with various Gaussian defect state densities positioned in CuO and Cu_2O band-gap, N_T(CuO) and N_T(Cu_2O), are presented in the Figure III.9.

When N_T(CuO) and N_T(Cu_2O) > 10^{16} cm^{-3}, the result depicts a negative influence on the device's performance. All the photovoltaic parameters, including V_{oc}, J_{sc}, FF, and η, are reduced. The carriers are trapped or recombined in flaws, resulting a waste of energy that does not contribute to the transportation of the current to the external load. When N_T(CuO) = 10^{15} cm^{-3}, a good performance was reached: J_{sc} = 24 mA/cm^2, V_{oc} = 0.90 V, FF = 85.65% and η = 19.21%. At a high defect concentration of around 3 × 10^{19} cm^{-3}, J_{sc} = 17 mA/cm^2, V_{oc} = 0.57 V, FF = 65% and η = 5%.

When N_T(Cu_2O) = 10^{15} cm^{-3}, a good performance of Cu_2O solar cell was reached: J_{sc} = 10.71 mA/cm^2, V_{oc} = 2.4 V, FF = 60% and η = 13%. At a high defect concentration of around 3 × 10^{19} cm^{-3}, J_{sc} = 9.18 mA/cm^2, V_{oc} = 9 V, FF = 19% and η = 9.1% were obtained. As a result, the bulk defect density, which is connected to creating trapping (recombination state) in the CuO and Cu_2O absorber bulk, may have a significant impact on current transport [22].

For a better understanding of current losses with increasing the defect concentration in the absorber bulk, the quantum efficiency QE was calculated and the results are given in Figure III.10 and Figure III.11. For wavelength below 500 nm and above 800 nm all samples show nearly the same behavior. In the region between 500 nm and 800 nm a significant loss is observable. When the defect concentration increases from 10^{14} cm^{-3} to 10^{19} cm^{-3} the maximum of quantum efficiency decreases significantly.

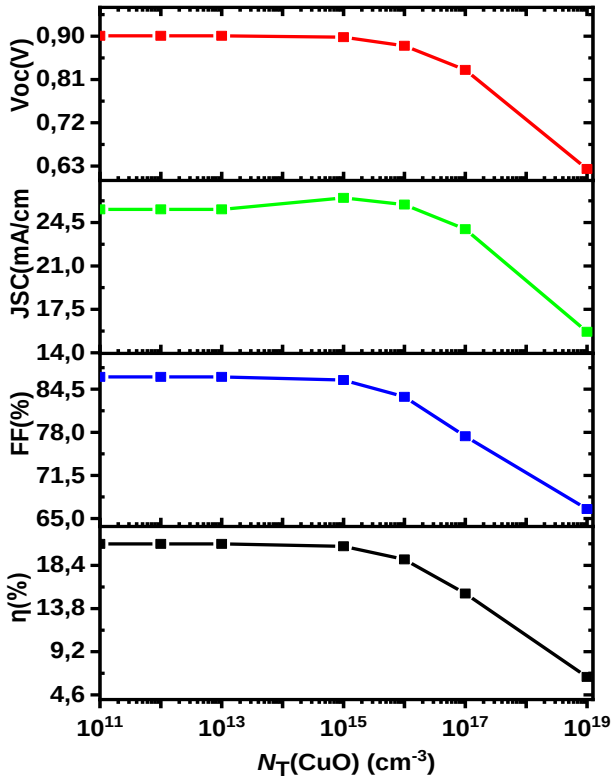

(a)

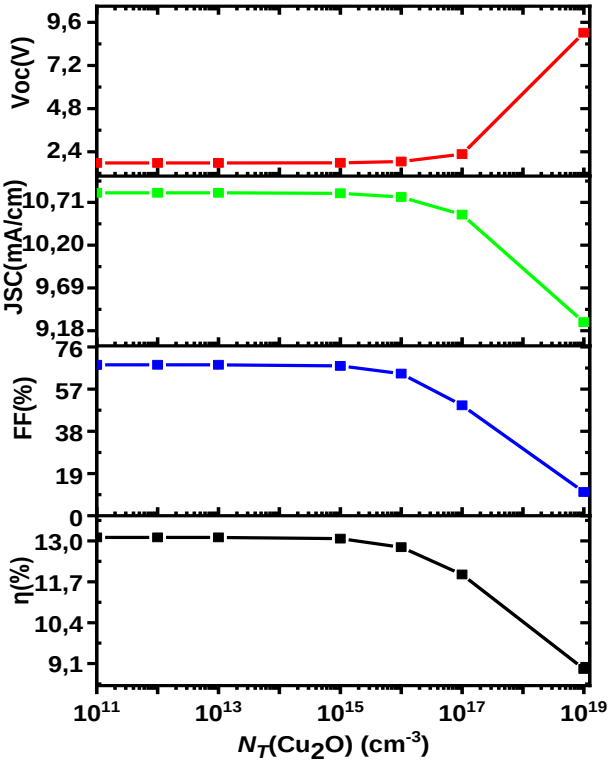

(b)

Figure III.9: Effect of defect density of (a) CuO and (b) Cu_2O absorber layer on the solar cell performances.

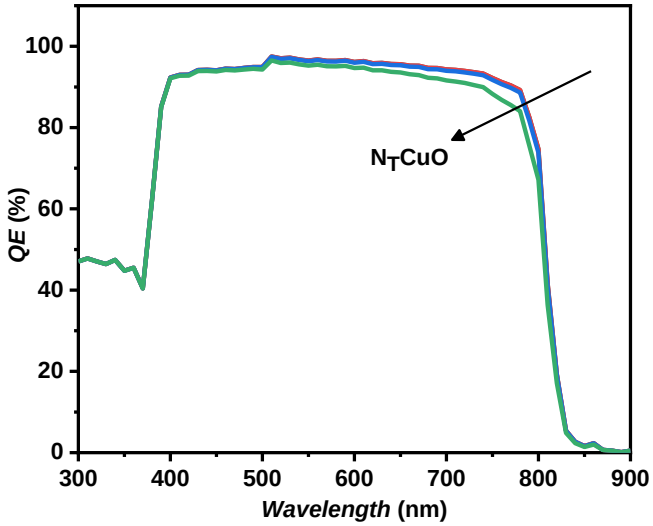

Figure III.10: Quantum efficiency versus wavelength of CuO solar cell with various N_T(CuO).

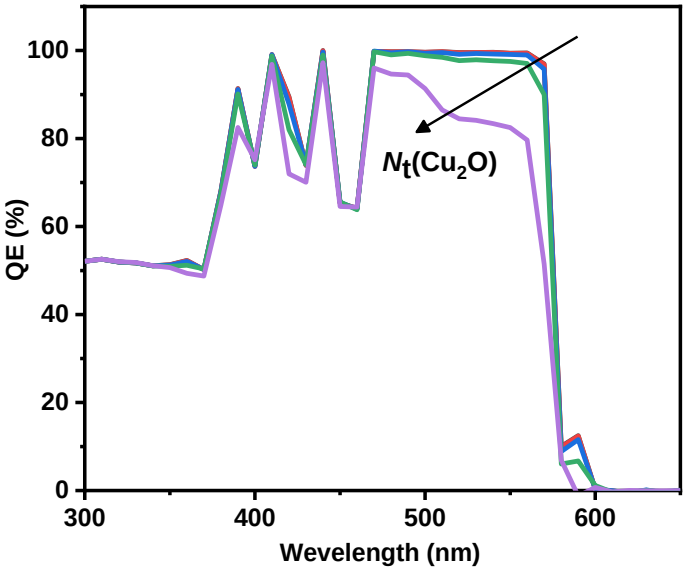

Figure III.11: Quantum efficiency versus wavelength of Cu_2O solar cell with various N_T(Cu_2O).

III.8. Hybrid CuO/CIGS and Cu_2O/CIGS solar cells modeling

To enhance light absorption and achieve high conversion efficiency, a variety of absorbers with various energy band gaps should be used. Figure III.12 depicts the CuO/CIGS and Cu_2O/CIGS and finally CuO/Cu_2O/CIGS Hybrid solar cells structural layout.

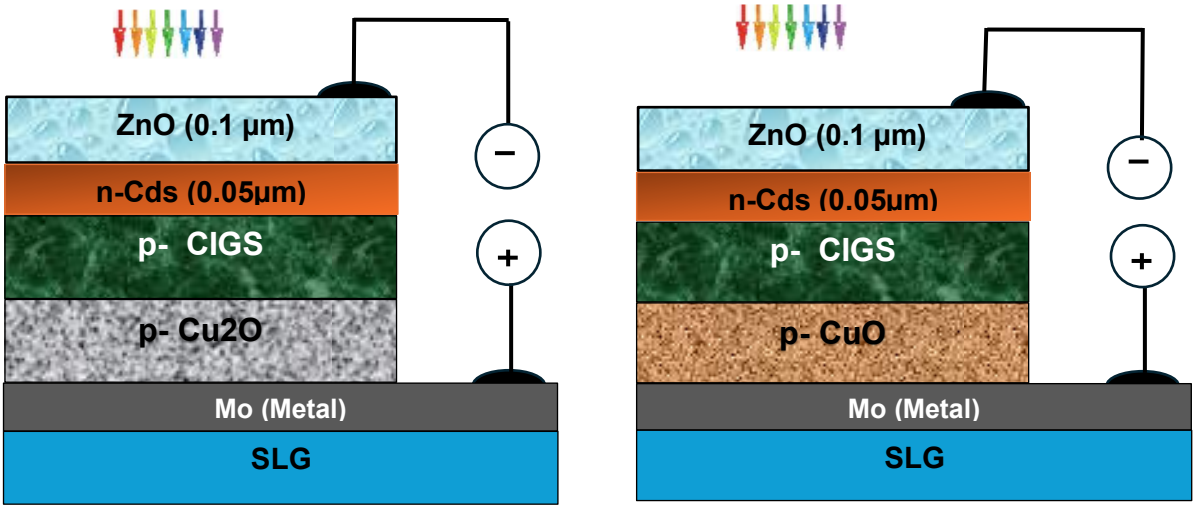

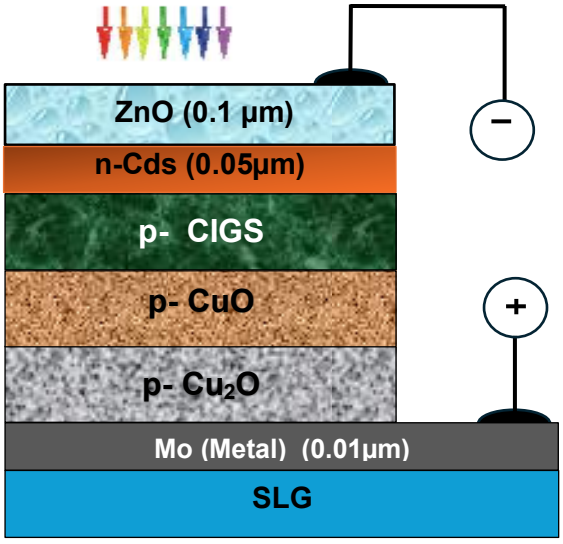

Figure III.12: Hybrid solar cells for different structures: (a) CuO/CIGS Hybrid solar cell, (b) Cu_2O/CIGS Hybrid solar cell and (c) CuO/Cu_2O/CIGS Hybrid solar cell structures.

Physical properties of the CIGS material, used in the simulation are available in data base of SCAPS-1 simulator. The parameters of CIGS, Cu_2O, CuO, CdS and ZnO used in our simulation are listed in Table III.2.

Table III.2: Parameters values of CIGS, CuO and Cu_2O materials used in the simulation.

Material properties	CuO	CIGS	Co_2O	CdS	ZnO
Thickness (µm)	3	To be varied	3	0.1	0.08
Band gap [eV]	1.51	1.2	2.17	2.4	3.3
Electron affinity [eV]	4.07	4.5	3.20	4.2	4.6
Dielectric permittivity (relative)	18.10	10	7.11	10	9
CB (conduction band) effective density of states [cm^{-3}]	2.2×10^{19}	2×10^{18}	2×10^{17}	2×10^{18}	2.2×10^{18}
VB (valence band) effective density of states [$1/cm^3$]	5.5×10^{20}	2×10^{18}	1.1×10^{19}	1.5×10^{19}	1.8×10^{19}
Electron mobility µn[cm^2 /Vs]	100	100	200	100	100
Hole mobility µp [cm^2 /Vs]	0.1	2.5	80	25	25
Shallow uniform donor density N_D [$1/cm^3$]	0	0	0	1×10^{17}	1×10^{19}
Shallow uniform acceptor density N_A [$1/cm^3$]	1×10^{16}	To be varied	1×10^{18}	0	0

III.8.1 Band diagrams

Figure III.13 exhibits the energy band diagrams for both (a) CuO/CIGS, (b) Cu_2O/CIGS and (c) Cu_2O/CuO/CIGS Hybrid solar cell structures obtained by simulation.

Depending on the solar cell structure and the absorber layers, i.e. the CuO and Cu2O layers onto CIGS absorber layer, a shift is observed as a stairs form in conduction band energy, this is beneficial for the collection of electrical charges. The influence of thickness, acceptor concentration and defect density of CIGS added layer on the CuO/CIGS and Cu2O/CIGS solar cells performances were obtained by following section.

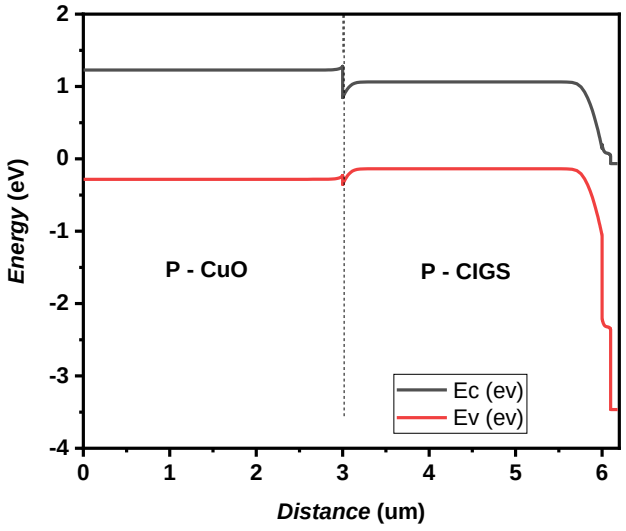

(a)

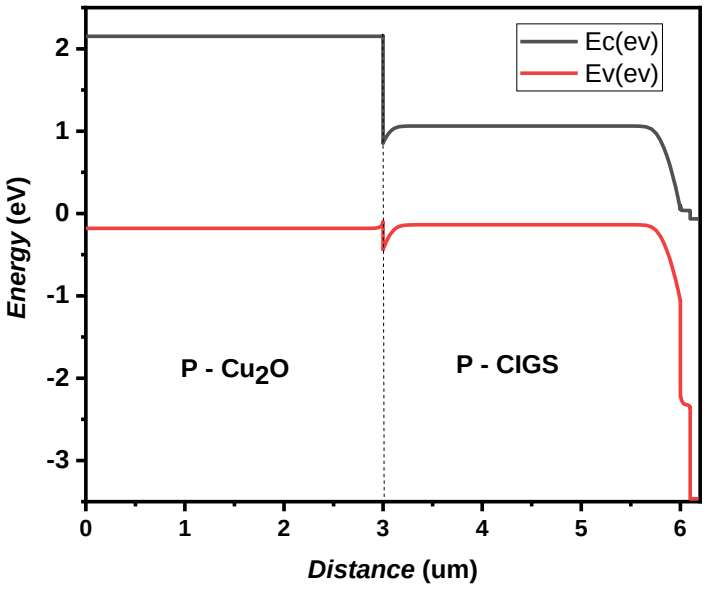

(b)

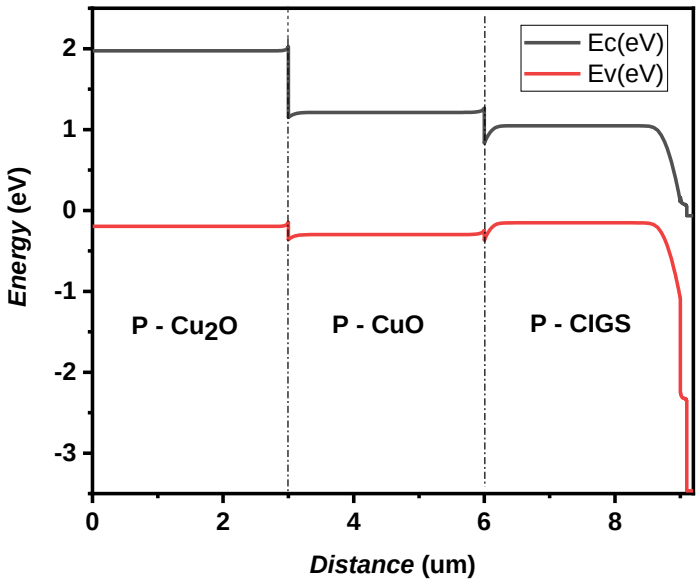

(c)

Figure III.13: Energy band diagrams for (a) CuO/CIGS, (b) Cu2O/CIGS and (c) Cu_2O/CuO/CIGS Hybrid solar cell structures obtained by simulation.

III.8.2 Thickness optimization of CIGS absorber layer for both structures

The thickness and acceptor concentration of p-CIGS absorber layer are found to be important parameters that directly influence the performances of Hybrid CIGS solar cells. Hence, at first, The CIGS absorber thickness has been varied to find the optimum thickness for high-performance Hybrid CIGS solar cells. The results (Figure III.14) indicate that the efficiency increased with the absorber thickness, t_{CIGS}, but with a much slower rate over 2 µm. The optimum thickness for CIGS absorber layer would be higher than 3 µm. From Figure III.14, at the thickness of 1 µm and 3 µm, the recorded efficiency is 16.66% and 19.12%, respectively. Comparing the results with the 18.39% efficiency at 2 µm, it was found out that a decrease in 1 µm of the absorber thickness resulted in 9.4% decrease in efficiency. On the other hand, increase in 1 µm of the absorber thickness only resulted in 3.8% increase in efficiency. A larger decrease can be observed below 1 µm. This calculation result agrees with the expected theoretical assumption that about 1-2 µm is sufficient to absorb most of the incident light. If the absorber layer thickness is reduced below 2 µm. The open circuit voltage (V_{oc}) and short circuit current density (J_{sc}) are increasing with the thickness of the absorber layer. This may mainly be due to the increase in the longer wavelengths absorption, which in turn contributes to electron-hole pair generation. We obtain a maximum fill factor of 78% when t_{CIGS} is higher than 2 µm.

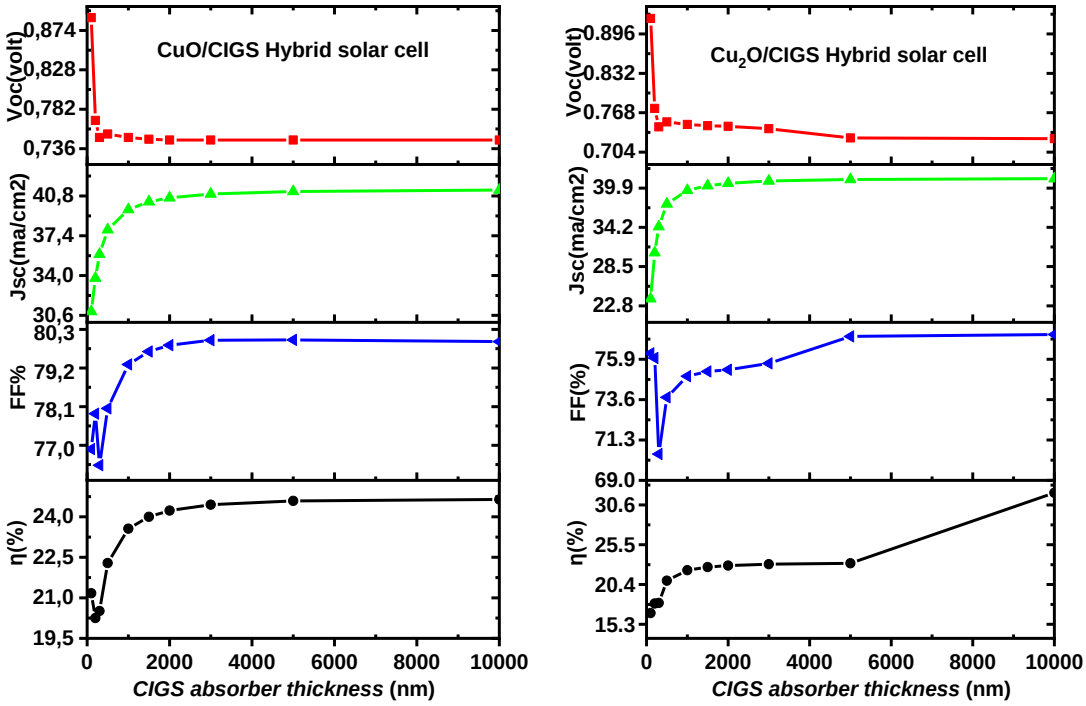

Figure III.14: Hybrid solar cell performance as a function of CIGS absorber layer thickness.

We can achieve a high efficiency of about 25.59% at $t_{CIGS} \approx 3$ µm with $FF = 79.4\%$, $V_{oc} = 0.74$ Volt and $J_{sc} = 40.11$ mA/cm^2 and about 22.52% at $t_{CIGS} \approx 3$ µm with $FF = 76\%$, $V_{oc} = 0.63$ Volt and $J_{sc} = 40.01$ mA/cm^2, for CuO/CIGS and Cu_2O/CIGS solar cells, respectively.

III.8.3 Optimization of acceptor density N_A(CIGS) for both structures

The acceptor concentration for absorber layer, N_A(CIGS), is varied from 10^{11} cm^{-3} to 10^{19} cm^{-3} and the simulated photovoltaic parameters are shown in Figure III.15. A higher acceptor concentration brings impact on electric field build-up within the space charge region. A higher electric field reduces the free carrier recombination, which basically increases V_{oc}. However, a higher value of N_A(CIGS) corresponds to an increase in the carrier recombination in the bulk, which thus reduces the magnitude of the short circuit current density. This phenomenon is observed in the J_{sc} vs. N_A(CIGS) plot of Figure III.14. Thus, the simulation reveals that a dominant rise in V_{oc} up to a tolerable limit of N_A(CIGS) would result in improving the efficiency. A small increase in FF occurs for N_A(CIGS) > 10^{13} cm^{-3} followed by a strong decrease for N_A(CIGS) > 10^{17} cm^{-3}. The maximum fill factor obtained is 84%. The results indicate that the efficiency η increases until it reaches a maximum around 24.13% and the N_A(CIGS) is required to be higher than 10^{16} cm^{-3} to obtain a good performance.

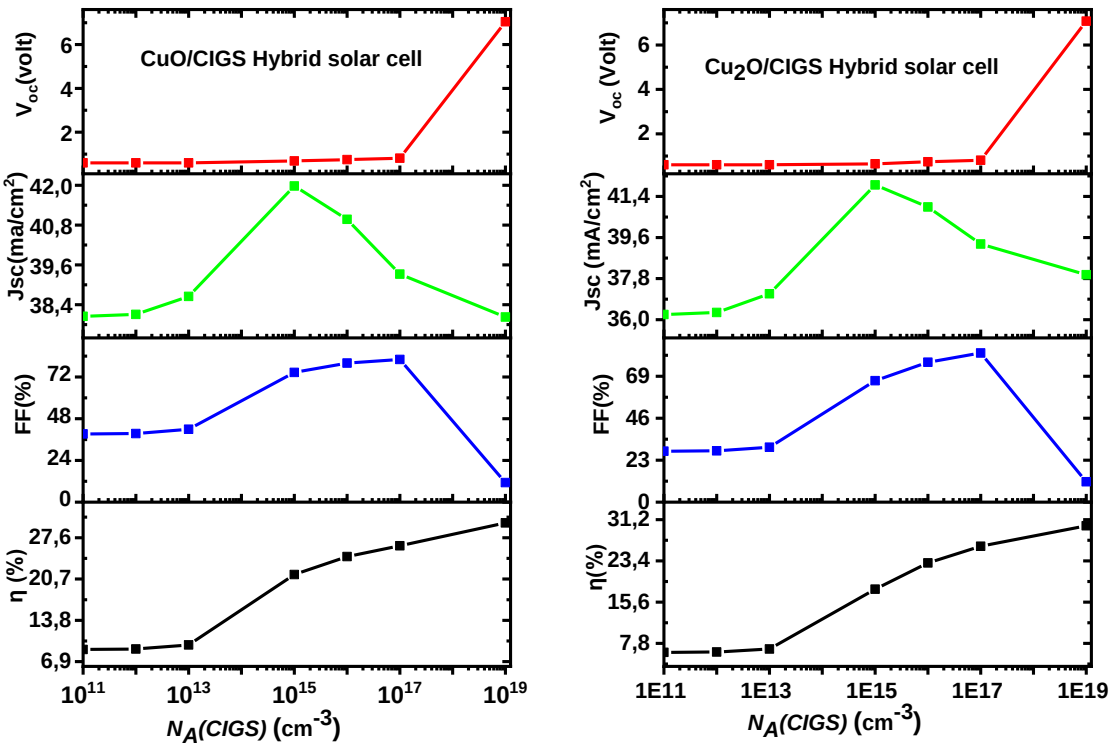

Figure III.15: Effect of acceptor concentration of CIGS absorber layer, N_A(CIGS), on Hybrid CuO/CIGS solar cell performance.

III.8.4 Influence of defect state density of CIGS absorber layer for both structures

The photovoltaic parameters corresponding to the J–V characteristics for front illumination as a function of defect state density, N_T(CIGS), of CIGS absorber layer are presented in Figure III.16. We can see that the defects state density up to 10^{13} cm^{-3} will cause efficiency reduction for this both kinds of Hybrid CIGS solar cells.

We can achieve the maximum efficiency of about 42.3% at N_T(CIGS) lower than 10^{13} cm^{-3} with FF = 47%, V_{OC} = 1.41 Volt, J_{SC} = 43.2 mA/cm^2 and about 39.5% with FF = 81.5%, V_{OC} = 1.02 Volt and J_{SC} = 42.1 mA/cm^2, for CuO/CIGS and Cu_2O Hybrid solar cells, respectively. It is obvious that at N_T(CIGS) = 10^{19} cm^{-3}, the cell has a poor performance with η= 7.05%, FF = 58.8%, V_{OC} = 0.41 V, J_{SC} = 35.6 mA/cm^2 for CuO/CIGS Hybrid solar cell, and with η= 6.8%, FF = 53.2%, V_{OC} = 0.39 V, J_{SC} = 42.2 mA/cm^2 for Cu_2O/CIGS Hybrid solar cell.

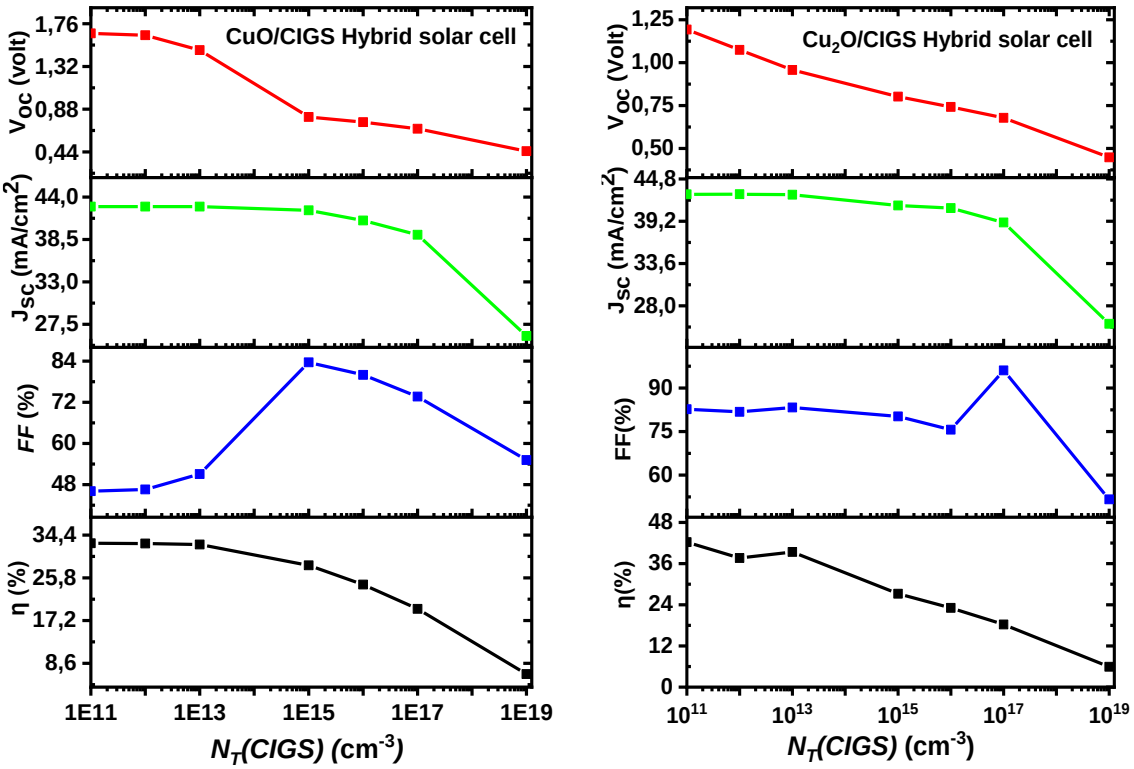

Figure III.16: Effect of defect density of CIGS absorber layer, N_T(CIGS), on Hybrid Cu_2O/CIGS and CuO/CIGS solar cells performances.

III.8.5 Study of Cu_2O/CuO/CIGS Hybrid solar cell as a function CIGS absorber layer thickness

Figure III.17 summarizes the effect of the CIGS absorber layer thickness (from 100 nm to 10000 nm) on the performance of the of Cu_2O/CuO/CIGS Hybrid solar cell. Because of its wide band gap of 2.51 eV for Cu_2O layer, 1.91 eV for CuO layer and 1.20 eV for CIGS absorber layers there are no considerable carriers generated in the CIGS absorber bulk. As expected for a thick CIGS absorber layer, from top to bottom, the J_{SC}, the Efficiency, the V_{OC} and the *FF* all showed fixed performance parameters of J_{sc} ~ 40.09 mA/cm^2, Efficiency ~ 20.81%, V_{OC} ~ 0.73 V and *FF* ~ 71.6%.

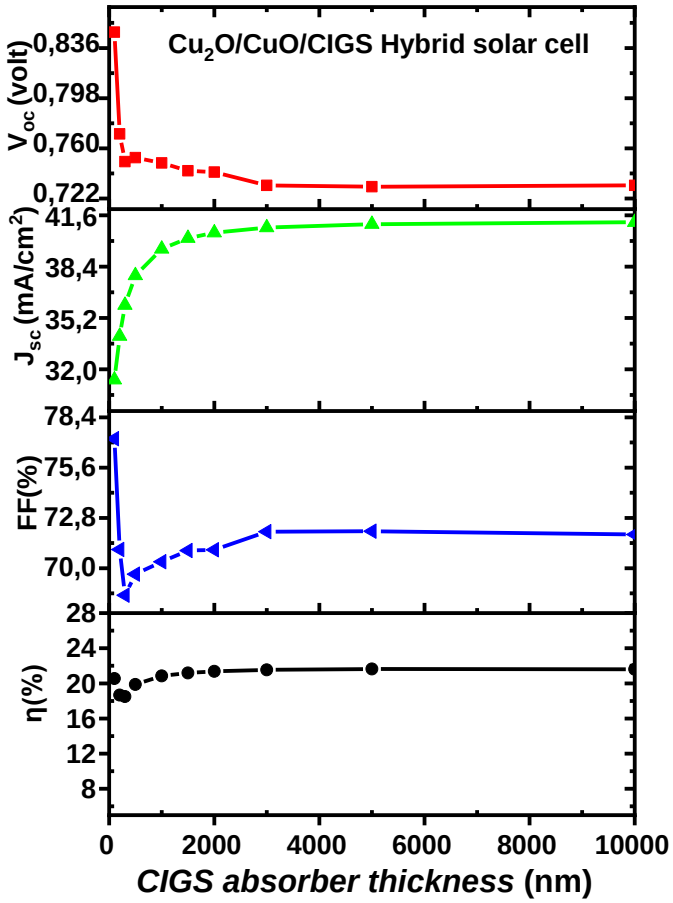

Figure III.17: Cu_2O/CuO/CIGS Hybrid solar cell performances as a function of CIGS absorber layer thickness.

III.9 Conclusion

The results of the present work at room temperature simulation for both Cu_2O and CuO solar cell are calculated using SCAPS-1D simulator, showing a good overall consistency for those listed in the literature. For both absorber layers, the performance parameters have been optimized for improving the performance of the Cu_2O and CuO thin film solar cells. Our results are in agreement with the high record conversion efficiency found experimentally of both solar cell structures. The absorber thickness, the acceptor concentration and the defect state density are optimized in this work. A good performance was obtained with an optimum thickness of about 3 μm for both Cu_2O and CuO thin films, the acceptor concentration, N_A(CuO) and N_A(Cu_2O) must be higher than 10^{16} cm^{-3} and lower than 1×10^{17} cm^{-3} and the defect state density N_T(Cu_2O) and N_T(CuO) must be lower than 10^{15} cm^{-3}.

Using SCAPS program, the optimized CuO and Cu_2O material parameters have been studied for improving the performance of the Hybrid CIGS thin film solar cell. Our results are in agreement with the high record conversion efficiency found experimentally for CuO/CIGS, Cu_2O/CIGS and Cu_2O/CuO/CIGS Hybrid solar cell structures. Through this work we can reduce the amount of precious materials (indium and gallium) use in CIGS absorber layer. Which is very promising and further improvements are possible for low cost Hybrid CIGS solar cells.

References

[1] Li Z, Tong K, Shi R, Shen Y, Zhang Y, Yao Z, Fan J, Thwaites M, Shao G 2017 Journal of Alloys and Compounds 695 3116-3123.

[2] Lu L, Guo M, Thornley S, Han X, Hu J H, Thwaites M J, Shao G, 2016 Sol. Energy Mater. Sol. Cells 149 310-319.

[3] Shen Y, Guo M, Xia X, Shao G 2015 Acta Materiala 85 122-131.

[4] Zou X W, Fan H Q, Tian Y M, Zhang M G, Yan X Y 2015 RSC Adv. 5 23401–23049.

[5] Sibiński M, Znajdek K 2011 Innovative elastic thin-film solar cell structures Solar Cells - ThinFilm Technologies (InTech) 253-274.

[6] Boudaoud L, Khelifi S, Mostefaoui M, Rouabhia A K, Sahouane N 2015 Energy Procedia 74 745- 751.

[7] Le Zhu Development of Metal Oxide Solar Cells through Numerical Modelling, PhD thesis.

[8] Minami T, Nishi Y, Miyata T, Nomoto J I 2011 Applied Physics Express Modeling Thin Film Solar Cells: From Organic to Perovskite. Advanced Science, 1901397.doi:10.1002/advs.201901397

[9] Ouédraogo, S., Zougmoré, F., Ndjaka, J. (2014). Computational analysis of the effect of the surface defect layer (SDL) properties on Cu (In, Ga) Se_2-based solar cell performances, J. Phys. Chem. Solids. 75 688-695.https://doi:10.1016/j.jpcs.2014.01.010.

[10] Pudov, A., Kanevce, A., Al-Thani, H. J. (2005). Secondary barriers in CdS-CuIn $_{1-x}Ga_xSe_2$ solar cells, J. Appl. Phys. 97, 064901.

[11] Bouabdelli, M. W., Rogti, F., Maache, M., Rabehi, A. (2020). Performance enhancement of CIGS thin-film solar cell. Optik. 216, 164948. .

[12] Wagner, S., Shay, J. L., Migliorato, P., Kasper, H. M. (1974). $CuInSe_2$/CdS heterojunction photovoltaic detectors. Applied Physics Letters. 25(8), 434-435. https://doi:10.1063/1.1655537.

[13] Inc. , Atlas User's Manual. Santa Clara, CA 95054, California (2017).

[14] Elbar, M., Tobbeche, S. (2015). Numerical Simulation of CGS/CIGS Single and Tandem Thin-film Solar Cells using the Silvaco-Atlas Software. Energy Procedia. 74, 1220-1227. https://doi:10.1016/j.egypro.2015.07.766.

[15] Repins, I., Contreras, M., Romero, M., Yan, Y., Metzger, W., Li, J., Noufi, R. (2008). Characterization of 19.9%-efficient CIGS absorbers. In 33rd IEEE Photovoltaic Specialists Conference (pp. 1-6). IEEE.https:

[16] Serin N, Serin T, Horzum S and Celik Y 2005 Semiconductor Science and Technology 20 398- 401.

[17] Amin G 2012 ZnO and CuO nanostructures: low temperature growth, characterization, their optoelectronic and sensing applications (1st ed. LiU-Tryck: Norrköping (Sweden)) [SE-601 74]

[18] Mohd Rafie Johan, Mohd Shahadan Mohd Suan, Nor Liza Hawari, Hee Ay Ching 2011 Int. J. Electrochem. Sci. 6 6094-6104.

[19] Abdu Y and Musa A O 2009 Bayero Journal of Pure and Applied Sciences 2(2) 8-12.

[20] Paulina Sawicka-Chudy, Grzegorz Wisz, Szymon Górny, Łukasz Głowa, Maciej Sibiński, Marian Cholewa Numerical simulation and analysis of experimental TiO2/Cu2O thin film for photovoltaic structures Journal of Nanoelectronics and Optoelectronics

[21] Jeong S S, Mittiga A, Salza E, Masci A, Passerini S 2008 Electrochim. Acta 53 2226-2231.

[22] Li B S, Akimoto K, Shen A 2009 J. Cryst. Growth 311 1102-1105.

[23] Lee Y S, Heo J, Winkler M T, Siah S C, Kim S B, Gordon R G, Buonassisi T 2013 J. Mater. Chem. A 1 15416.

[24] Hossain M I, Alharbi F H 2013 Mater. Technol.: Adv. Perform. Mater. 28 88-97.

[25] Hossain M I, Alharbi F H, Tabet N 2015 Solar Energy 120 370-380.

[26] Rivera R, Stashans A 2013 Defects in TiO2 Crystals Proceedings of the International MultiConference of Engineers and Computer Scientists (Vol II, IMECS, March 13 - 15, 2013, Hong Kong).

[27] Kars I, Cetin S S, Kınacı B, Sarıkavak B, Bengi A, Altuntas H, Ozturk M K and Ozcelik S 2010 Surf. Interface Anal. 42 1247-1251.

[28] Li B S, Akimoto K, Shen A 2009 J. Cryst. Growth 311 1102-1105.

[29] Xosrovashvilia G, Gorjib N E 2013 J. Mod. Opt 60 936–940.

[30] Gou L, Murphy C J 2003 Nano Lett. 3 231-234. [42] Wang W Z, Wang G H, Wang X S, Zhan Y J, Liu Y K , Zheng C L 2002 Adv. Mater. 14 67-69.

[31] Liao L, Yan B, Hao Y F, Xing G Z, Liu J P, Zhao B C, Shen Z X, Wu T, Wang L, Thong J T, Li C M, Huang W, Yu T 2009 Appl. Phys. Lett. 94.

[32] Scanlon D O, Morgan B J, Watson G W 2009 J. Chem. Phys. 131.

[33] Zhu L, Shao G, Luo J K 2011 Semicond. Sci. Technol. 26.

[34] Korzhavyi P A, Johansson B 2011 Literature review on the properties of cuprous oxide Cu2O and the process of copper oxidation Technical Report TR-11-08

[35] Matsumura H, Fujii A, Kitatani T 1996 Jpn. J. Appl. Phys. 35.

[36] Paulina Sawicka-Chudy, Maciej Sibiński, Grzegorz Wisz Elżbieta Rybak-Wilusz, Marian Cholewa 2017 Numerical Analysis and Optimization of Cu2O/TiO2, CuO/TiO2, Nanostructures PV using SCAPS Proceedings International Conference on Microtechnology and Thermal Problems in Electronics MICROTHERM 71-72.

[37] Lee S H, Yun S J, Lim J W 2013 The Characteristics of Cu2O Thin Films Deposited Using RFMagnetron Sputtering Method with Nitrogen-Ambient ETRI J. 35.

[38] Ritter E 1975 Phys. Thin Films 8.

[39] Liangbin Xionga, Sheng Huanga, Xi Yanga, Mingqiang Qiuc, Zhenghua Chena, Ying Yua, 2011 Electrochimica Acta 56(6) 2735-2739.

[40] Jun-Yong Parka, Chan-Soo Kimb, Kikuo Okuyamac, Hye-Moon Leed, Hee-Dong Jange, SungEun Leef, Tae-Oh Kima 2016 Journal of Power Sources 306 764-771.

[41] Masaya Ichimura, Yoshihito Kato 2013 Materials Science in Semiconductor Processing 16(6) 1538-1541.

[42] G. Kresse and D. Joubert, Phys. Rev. B 59, 1758 (1999).

[43] J. F. Pierson, A. Thobor-Keck, and A. Billard, Appl. Surf. Sci. 210, 359 (2003).

[44] M. Heinemann, B. Eifert, and C. Heiliger, Phys. Rev. B 87, 115111 (2013).

[45] L. Y. Isseroff and E. A. Carter, Phys. Rev. B 85, 235142 (2012).

[46] F. Bruneval, N. Vast, L. Reining, M. Izquierdo, F. Sirotti, and N. Barrett, Phys. Rev. Lett. 97, 267601 (2006)

[47] F. Bruneval, N. Vast, L. Reining, M. Izquierdo, F. Sirotti, and N. Barrett, Phys. Rev. Lett. 97, 267601 (2006).

General conclusion

General conclusion

In this work, we studied the electrical characteristics of the ZnO/CdS/CuO and ZnO/CdS/Cu_2O heterojunction solar cells. High doped n-type ZnO layer is a TCO layer used as a window layer which allows light to pass through with minimal reflection, the n-type CdS buffer layer creates the p-n junction with the p-CuO and p-Cu_2O absorber layers. To simulate these solar cell structures we used SCAPS-1D digital simulation software. The solar cell structures are subjected to AM1.5G illumination and an operating temperature of 300K were used. The current-voltage electrical characteristics of the solar cells were calculated for each variation in parameters of the thin layers constituting the cells. From these electrical characteristics we can derive four photovoltaic parameters defining the structure, such as: the short-circuit current density (J_{SC}), the open-circuit voltage (V_{OC}), the fill factor (FF) and the photovoltaic conversion efficiency (η).

These characteristics are studied and analyzed under the variation of several physical and geometric parameters, such as: the thickness of the p-CuO and p-Cu_2O absorber layers, the concentration of acceptors N_A(CuO) and N_A(Cu_2O) and the density of defects N_T of the heavily p-doped CuO and p-Cu_2O absorber layers.

It turns out that changes made to the geometrical properties of the two structures based on p-CuO and p-Cu_2O absorbers, the thickness of CuO and Cu_2O absorber layers, generally have a very significant effects on the electrical characteristics of the cell compared to the changes made to the properties of the CdS or ZnO layers. The optimal thicknesses of both absorbers are 3 µm.

We can say that the electronic characteristics of the solar cell based on CuO and Cu_2O absorbers closely depend on the physical parameters such as: acceptor concentration (N_A) and/or defects concentration (N_T) of both absorbers. The optimum performances were obtained with $10^{16} \leq N_A \leq 10^{17}$ cm^{-3} and $N_T \leq 10^{15}$ cm^{-3}. The results obtained by the SCAPS simulator are satisfactory and are in agreement with the published results.

A hybrid solar cells is the combination of CuO and/or Cu_2O absorber layers with CIGS photovoltaic technologies in a single solar cell structure. Firstly, CuO/CIGS and Cu_2O/CIGS solar cells are installed separately, emerges the hybrid solar cells, capable of simultaneously generating electricity with high conversion efficiency. This is due to the ability of the hybrid solar cells to be able to take advantage of the entire spectrum of existing light. The optimum performances of about 25.8% and 22.6% were obtained with a minimum thickness of CIGS absorber of 2 µm for CuO/CIGS and Cu_2O/CIGS structures, respectively. The calculation indicates that the optimum performances were obtained with $10^{15} \leq N_A(CIGS) \leq 10^{17}$ cm^{-3} and $N_T(CIGS) \leq 10^{13}$ cm^{-3} for both structures.

Secondly, Cu_2O/CuO/CIGS solar cells is then installed, emerges the good heterojunction solar cells, we found that there was no considerable effect of the CIGS layer on the cell performance.

This simulation work opens the way to new perspectives in the photovoltaic field with potential applications in the field of photovoltaic conversion. We suggest: a) comparing the results obtained by the one-dimensional SCAPS simulator by others using two oe three dimensional software, such as SILVACO/Atlas, b) Fabricate the complete ZnO/CdS/CuO, ZnO/CdS/Cu_2O and the Cu_2O/CuO/CIGS photovoltaic cell.

Abstract

In the global context of the diversification of the use of natural resources, the use of renewable energies and in particular solar photovoltaics is becoming increasingly strong. As such, the development of a new generation of photovoltaic cells based on CuO and Cu_2O seems promising. In fact, the yield of these cells has exceeded 20% in recent years with certain development conditions. In this simulation work, we used very powerful software that is very suitable for the type of our solar cell, called SCAPS-1D. The use of this tool allowed us to study the performance of ZnO/CdS/CuO and ZnO/CdS/Cu_2O solar cells. The geometrical and physical parameters were studied and their influence on the cell performance were determined. The Hybrid CIGS solar cell structures including CuO and/or Cu_2O absorber layers were optimized.

Keywords: Solar cell, thin films, CuO and Cu_2O absorber layers, simulation, SCAPS-1D.

ملخص

في السياق العالمي لتنويع استخدام الموارد الطبيعية، أصبح استخدام الطاقات المتجددة، وخاصة الطاقة الشمسية الكهروضوئية، قويا بشكل متزايد. على هذا النحو، فإن تطوير جيل جديد من الخلايا الكهروضوئية المعتمدة على CuO و Cu_2O يبدو واعدًا. وفي الواقع، تجاوز إنتاج هذه الخلايا 20% في السنوات الأخيرة مع ظروف نمو معينة. في عمل المحاكاة هذا، استخدمنا برنامجًا قويًا جدًا ومناسبًا جدًا لنوع خليتنا الشمسية، يسمى SCAPS-1D. أتاح لنا استخدام هذه الأداة دراسة أداء الخلايا الشمسية ZnO/CdS/CuO و ZnO/CdS/Cu_2O. تمت دراسة العوامل الهندسية والفيزيائية وتحديد تأثيرها على أداء الخلية. تم تحسين هياكل الخلايا الشمسية Hybrid CIGS بما في ذلك طبقات امتصاص CuO و/أوCu_2O .

الكلمات المفتاحية: الخلايا الشمسية، الأغشية الرقيقة، الطبقات الممتصة لأكسيد النحاس و ثنائي أكسيد النحاس، المحاكاة، SCAPS-1D.

Résumé

Dans le contexte mondial de diversification de l’usage des ressources naturelles, le recours aux énergies renouvelables et notamment au solaire photovoltaïque devient de plus en plus fort. A ce titre, le développement d’une nouvelle génération de cellules photovoltaïques à base de CuO et Cu_2O semble prometteur. En effet, le rendement de ces cellules a dépassé les 20 % ces dernières années avec certaines conditions de développement. Dans ce travail de simulation, nous avons utilisé un logiciel très puissant et très adapté au type de notre cellule solaire, appelé SCAPS-1D. L'utilisation de cet outil nous a permis d'étudier les performances des cellules solaires ZnO/CdS/CuO et ZnO/CdS/Cu_2O. Les paramètres géométriques et physiques ont été étudiés et leur influence sur les performances des cellules a été déterminée. Les structures de cellules solaires hybrides CIGS comprenant des couches absorbantes de CuO et/ou Cu_2O ont été optimisées.

Mots clés : Cellule solaire, couches minces, couches absorbantes CuO et Cu_2O, simulation, SCAPS-1D.